

April 2013

Toward a Biologically Inspired Human-Carrying Ornithopter Robot Capable of Hover

Bo Rim Seo

Worcester Polytechnic Institute

Nicholas Deisadze

Worcester Polytechnic Institute

Woo Chan Jo

Worcester Polytechnic Institute

Follow this and additional works at: <https://digitalcommons.wpi.edu/mqp-all>

Repository Citation

Seo, B. R., Deisadze, N., & Jo, W. C. (2013). *Toward a Biologically Inspired Human-Carrying Ornithopter Robot Capable of Hover*. Retrieved from <https://digitalcommons.wpi.edu/mqp-all/876>

This Unrestricted is brought to you for free and open access by the Major Qualifying Projects at Digital WPI. It has been accepted for inclusion in Major Qualifying Projects (All Years) by an authorized administrator of Digital WPI. For more information, please contact digitalwpi@wpi.edu.

Toward Biologically Inspired Human-Carrying Ornithopter Robot Capable of Hover

April 2013

A Major Qualifying Project Report

Submitted to the Faculty of the

Worcester Polytechnic Institute

In partial fulfillment of the requirements of the

Degree of Bachelor of Science

By

Nicholas Deisadze

Woo Chan Jo

Bo Rim Seo

Prof. Marko B. Popovic, Major Advisor

Prof. Stephen S. Nestinger, Co-Advisor

Abstract

Since dawn of time humans have aspired to fly like birds. However, human carrying ornithopter that can hover by flapping wings does not exist despite many attempts to build one. This motivated our MQP team to address feasibility of heavy weight biologically inspired hovering robot. To this end, aerodynamics of flapping wing flight was analyzed by means of an analytical model and numerical simulation, and validated through physical experiments. Two ornithopter prototypes were designed, constructed and evaluated under repeatable lab conditions. A small-scale ornithopter design, weighing 2.0 kg with a 1.2 m wingspan flapping at 2.5 Hz flapping frequency, was designed with a crank-rocker drive mechanism having wings with integrated flaps for reduced upstroke induced drag. This model was activated on a force plate to measure the lift forces. Due to a low signal-to-noise ratio, this experiment was unable to validate our theoretical model. A large-scale ornithopter design, weighing 22 kg with a wing span of 3.2 m flapping at 4 Hz flapping frequency, used a spring-based drive mechanism to enhance power output during downstroke. The large-scale ornithopter was tethered to a spring and activated while data were gathered with high-speed video camera. Results from these experiments agreed with our theoretical prediction. Interestingly, our power requirement study show that ornithopters can be more advantageous compared to fixed wing and rotary blade aircraft. With high maneuverability, a large range of possible speeds, and reduced power requirements, ornithopters may be a viable and attractive mode of transportation that deserves more dedicated research and practical realizations

Acknowledgments

The authors would like to thank Thane Hunt and Phillip O’Sullivan for their help without which this project would not be brought into completion. The authors would also like to thank the WPI Mechanical Engineering, Biomedical Engineering, and Physics Departments for research funding and Maxon Motors for generous support.

Table of Figures

Figure 1: The muscle groups of a bird.	7
Figure 2: The Objectives Tree created to organize the project	15
Figure 3: The fully assembled small-scale prototype design	24
Figure 4: CAD drawing of the small-scale prototype design.....	25
Figure 5: The valve mechanism for flapping wings.	26
Figure 6: Diagram of the first prototype transmission system and wings.....	26
Figure 7: The design of the large-scale prototype.....	28

Table of Tables

Table 1: Pairwise Comparison Chart.	17
--	----

Table of Contents

Abstract	ii
Acknowledgments.....	iii
Table of Figures	iv
Table of Tables	iv
Chapter 1: Introduction.....	1
Chapter 2: Literature Review.....	3
2.1 Successful Ornithopters	4
2.2 Flight Types	5
2.2.1 Flapping Wing Flight.....	5
2.2.2 Fixed Wing Flight.....	6
2.3 Bird Flight Biomechanics	6
2.3.1 Muscles Involved in Bird Flight	7
2.3.2 Feathers and Their Effect on Flight	8
2.3.3 Dynamics of Wing Motion during Flight.....	9
2.4 Aerodynamics of Flapping Wing Flight	11
Chapter 3: Project Strategy	14
3.1 Initial Client Statement	14
3.2 Revised Client Statement.....	14
3.3 Objectives	15
3.3.1 Cost	16
3.3.2 Durability.....	16
3.3.3 Safety	16
3.3.4 Weight.....	16
3.3.5 Manufacturability.....	16
3.3.6 Effectiveness	17
3.3.7 Easy to Operate	17
3.3.8 Pairwise Comparison Chart	17
3.3.9 Constraints	18
3.4 Project Approach.....	18
Chapter 4: Design and Analysis.....	21

4.1	Needs Analysis.....	21
4.2	Power Analysis: Flapping Wing and Fixed Wing Flight	21
4.3	Functions and goals.....	22
4.4	Conceptual Designs and their Specifications	23
4.5	Analytical Theoretical Flapping Flight Model.....	23
4.6	Small-Scale Prototype Design	23
4.6.1	Design and Manufacturing.....	24
4.6.2	Wing Design	25
4.6.3	Drive Mechanism.....	26
4.6.4	Experiment.....	27
4.6.5	Small-Scale Prototype Design Summary	27
4.7	Large-Scale Model Design.....	28
4.7.1	Manufacturing.....	29
4.7.2	Drive Mechanism.....	29
4.7.3	Simulation	30
4.7.4	Experiments	31
4.8	Design Summary.....	31
Chapter 5:	Results and Discussion.....	32
5.1	Experiments: Performance and Results	32
5.1.1	Small-Scale Prototype Experiments.....	32
5.1.2	Large-Scale Prototype Experiments.....	32
5.2	Discussion	33
5.2.1	Feasibility Study and Theoretical Model Validation	34
5.2.2	Final Design Testing	34
5.2.3	Economic Considerations	34
5.2.4	Environmental Impact.....	34
5.2.5	Societal Impacts	35
5.2.6	Political Impacts.....	35
5.2.7	Manufacturability.....	35
5.2.8	Sustainability.....	35
Chapter 6:	Conclusions and Recommendations.....	36

6.1	Conclusions.....	36
6.2	Recommendations.....	36
	References	38
	Appendix A: Detailed Calculations	43
	A.1 More detailed calculation.....	43
	Appendix B: General Flapping Theory.....	44
	B.1 Model Dependent Dynamics.....	45
	B.2 Quick Estimation of Forces and Moments for the Second Prototype	48
	B.3 Calculation of Spring Engagement Duration	50
	Appendix C: Source Code	52
	D.1 Simulation Matlab Code	52
	Appendix D: Design Matrix.....	54
	Appendix E: Analytical Stress Analysis	55
	E.1 Stress Analysis for the Large-Scale Prototype Wings.....	55
	E.2 Analytical Fatigue Stress Analysis of the Reinforced Wing Design	57
	Appendix F: CAD Drawings	60
	F.1 CAD Drawings of the Small-Scale Prototype	60
	F.2 CAD Drawings of the Large-Scale Prorotype and Other Parametric Simulations	62
	Appendix G: Alternative Designs Generated during the Design Process.....	66
	G.1 Conceptual design with rotating platform using universal joint	66
	G.2 Second prototype with proposed counter balance.....	66
	G.3 Proposal for the first prototype	68
	G.4 Gigantic Flapping Wing Robot.....	70
	G.5 Proposal for second prototype.....	73

Chapter 1: Introduction

Flapping wing flight has numerous advantages over conventional fixed wing or rotor wing flight. In many cases, birds can attain near vertical takeoff, perform agile dynamic maneuvers, fly at rather slow speeds, and use environmental conditions via intelligent flapping, soaring, and gliding in a highly energy efficient manner (Shyy *et al.*, 1999). Imagine an aircraft that can mimic a bird. Based on energy considerations, the team proposed that flapping wing aircraft, i.e. ornithopters, are capable of carrying human occupants and may perform better than any hybrid system represented by similarly classed fixed-wing aircraft potentially integrated with helicopter rotor blades.

In actuality, flapping wing aircraft can perform on par with conventional fixed-wing aircraft. However, the added wing actuation enhances maneuverability, and may achieve novel functionality (Barry *et al.*, 2013). This includes hovering and flying with substantially lower energy requirements. There have been numerous attempts of building flapping wing machines in the past (Barry *et al.*, 2013; Brooks, 1985; DeLaurier, 1993, 1999, 2005; Deubel, 2007; Hunt *et al.*, 2005; Kim, 2006, 2009; Lin *et al.*, 2006; Mazaheri, 2010; Regan *et al.*, 2006) and while no fundamental obstacle exists in developing a hovering ornithopter capable of carrying a human, such aircraft have yet to be successfully designed and created. In contrast, simpler vehicles like helicopters and quadcopters can hover, maneuver, and carry large weights while there has not been a single example of large birdlike robot hovering at zero speed.

Groups at MIT (Smart Bird, 2011) and Festo (Send *et al.*, 2012) have recently built working examples of biologically inspired flapping birdlike robots. Festo's Smartbird has a wingspan of 2 meters and weighs 450 grams. The wings passively bend to exert thrust forces during both the upstroke and downstroke. MIT's Phoenix can carry up to 400g of cargo and is mainly designed for controls research (Subbaraman, 2009). However, these models still require some forward speed or appropriate head wind to fly. The same is true for all commercially available ornithopters and flying robots developed at other research labs (Jackowski, 2009)

Successful hovering at zero speed was recently achieved with small hummingbird robots (Dashevsky, 2011) and a new generation of insect-like Micro Aerial Vehicles (MAVs) (Shyy *et al.*, 1999). This class of flyers may have viable application in intelligence, surveillance, and reconnaissance missions (Baek *et al.*, 2011). Moreover, MAVs are also utilized to study the aerodynamics of biologically inspired flying (Paranjape, 2012).

With a focus on transportation and eventual goal to build a fully autonomous robotic flyer capable of carrying 100 kg, this paper reports on the development of a, 20 kg, biologically inspired

ornithopter robot which was preceded by lighter 2kg prototype for proof-of concept testing. The larger model is a second robot in this series that cannot fly on its own but can be utilized to study actuation mechanisms, various wing designs, flapping strategies and sensory motor control.

Our wing designs use some of the basic principles observed in nature. For example, a bird's wing is far more complex in its function than conventional an aircraft's wing. During the downstroke, the feathers of many bird species stay together to form a smooth, solid surface whereas during an upstroke, the feathers bend and spread to allow air flow between them (Biewener, 2011). Similarly, our designs explore air flux through wings to reduce drag during the upstroke.

Our advanced flapping mechanism utilizes the One-To-Many (OTM) principle (Hunt *et al.*, 2012, 2013) where the motor never directly engages the wing during the lift generating downstroke. Instead, the motor slowly builds up energy in the wing elastic element during the slow upstroke. The elastic element is then released from the motor, allowing for a fast downstroke. Hence, the power output can be multiple times larger than the power input. There is no need for the motor to passively hold the wing since the wing elastic element is already in a pre-tensed condition while the wing is at its lowest angular displacement and supported by a stopper. Since the motor is disengaged from wing during the powerful downstroke, no unexpected (motor damaging) drag induced torques can be encountered. Furthermore, due to pre-known condition (i.e. wing spring constant and elongation) the motor may always rotate in same direction at a torque and velocity optimum to its performance curves.

The sensory motor control is crucial for ornithopter robots. Manual flying of ordinary planes or helicopters is a non-trivial task. Manual flying of complex ornithopters with many degrees of freedom might be an impossible task, especially if maximum energy efficiency and/or maneuverability are required. The design team consisting of WPI students and professors involved in this project envisions that a human operator may provide only maneuvering commands while the robotic system handles flight stability. Robotic commands should be based on rapidly changing sensory information including 12-variables global state vector (6 per position and orientation spaces), internal state vector (i.e. proprioception), pressure, temperature, wind, water concentration, and localization of possible obstacles on flyer's path.

Chapter 2: Literature Review

The dream of feasible heavier than air flight only recently came to fruition in the early 20th century. Flight using air balloons has been possible since 1783 and the Lilienthal brothers accomplished a gliding flight towards the end of 19th century. It was the Wright brothers who eventually accomplished the first powered flight with a machine using fixed wings in 1903. It is a little known fact that many attempts had been made in past to fly with flapping wings like birds do (Anderson, 2002). One of the first known birdlike flight examples comes from the Greek myth of Icarus. Daedalus, father of Icarus, constructed wings from feathers and wax and together they tried to escape imprisonment from the King of Crete. Legends say that in the early 11th century, a monk named Eilmer in the abbey at Malmsbury had successfully flown using fastened wings on his hands. Historian reports that Eilmer flew six hundred feet after he jumped off the tower, but he was soon cast down by violent winds and broke his legs, remaining a cripple for the rest of his life. Following Eilmer, many more individuals tried to fly throughout the middle ages using wings attached to their hands, but most of them were either seriously or fatally injured due to their chosen modes of flight (Anderson, 2002; Singer, 2003; Torenbeek *et al.*, 2009).

During the Renaissance, Leonardo da Vinci (1452- 1519), inspired by his observations on birds, also tried to design a flying machine. Da Vinci came up with a human powered ornithopter design that never worked due to its heavy mass and inefficient energy provided by human power. Following this design, scientists in 1600s observed that human power alone would not be able to power a flying machine. More precisely, Giovanni Borrelli, father of biomechanics noted in one of his published papers that humans did not have enough muscle strength to fly and that birds had much larger muscle power to body weight ratio than humans did. Nonetheless, throughout the 17th and 18th centuries, scientists and engineers were coming out with different human powered ornithopter designs that never worked. Robert Hooke (1635-1703), a British physicist, claimed that he was able to fly using an ornithopter, but he noted that it was difficult to remain airborne (Anderson, 2002; Singer, 2003; Torenbeek *et al.*, 2009).

At the end of the 19th century, the Lilienthal brothers followed the idea of gliding and tried to build a successful ornithopter. To accomplish this, they investigated and observed bird flight extensively. The Lilienthal brothers observed that birds mainly flap their wings for propulsion and that flying does not fully depend on flapping alone, but on gliding as well. Therefore, they abandoned their idea of powered flight and turned their focus towards gliding. The Lilienthal brothers built the first carbon dioxide engine powered ornithopter. However, it did not achieve successful flight. Sir George Cayley (1773-1857) was an engineering pioneer that directed heavier than air flight away from flapping wing mechanisms. He

noted that due to complexity, flapping wing design should be forgotten and fixed wing flight and propulsion should be taken into consideration instead (Anderson, 2002; Singer, 2003; Torenbeek *et al.*, 2009).

Scientists and engineers following Cayley's ideas put ornithopters aside and concerned themselves with fixed wing flying mechanisms. However, ornithopters still remained in the interests of other researchers who tried building successful models. For example, in 1870, Alphonse Penaud came up with rubber-powered ornithopters that performed powered glides (Slaboch, 2002). In the same time frame, in France, Gustav Trouve constructed and flew an ornithopter for 70 m before the French Academy of Science. In 1890, Lawrence Hargrave, a British aeronautical pioneer constructed steam and compressed air powered ornithopters (Sterchak, 2009). Alexander Lippish a German engineer designed, built, and successfully flew ornithopters in 1930s (DeLaurier, 1994). More recently, James DeLaurier and his team at University of Toronto designed and built a successful ornithopter. In 1991 DeLaurier's team tested a prototype which was able to fly after it was launched by hand. In 1999, DeLaurier and colleagues tested a full scale, human piloted ornithopter which was able to fly independently using power generated from flapping wings alone and achieved 45 mph forward thrust (Slaboch, 2002). Nowadays, even though, there has been some interest and achievement in human flight using flapping wings, most ornithopters are miniature sized and used for applications such as hobbies, military and civil surveillance missions. This increased interest in miniature ornithopters is largely due to smaller scale ornithopters displaying advantages over the same size fixed wing flight machines. Namely, miniature ornithopters require less mass and energy to generate lift and thrust due to the flapping action of wings (Mueller, 2001).

2.1 Successful Ornithopters

An ornithopter is a device that flies by flapping its wings. The word "ornithopter" (c.1908) combines the ancient Greek words for "bird" and "wing". The first successful flight of a manned ornithopter took place in 1942. Adalbert Schmid's engine-powered manned ornithopters, flown in 1942 and 1947, were the most successful to date. The recent "bird-man suit" video with "flying" Dutchman Jarno Smeets that went viral on the Internet proved to be a hoax (BBC News, 2012; The Ornithopter Zone, 2012).

One of the first ornithopters was constructed by Gustave Trouvé in 1870. It used an unusual type of internal combustion engine; twelve gunpowder charges were fired successively into a bourdon tube to flap the wings. The Bourdon pressure gauge uses the principle that a flattened tube tends to change to be

straightened or larger circular cross-section when pressurized. Eugene Bourdon patented his gauge in France in 1849. This ornithopter flew 70 meters in a demonstration for the French Academy of Science (cyberneticzoo.com, 2012; The Ornithopter Zone, 2012).

Modern ornithopters like the ones constructed in 2007 by Robert Musters use actively twisted wings made of foam. The appearance of these radio-controlled ornithopters is close to that of a real bird and they are being offered for use in bird control at airports (Diaz, 2012; The Ornithopter Zone, 2012).

In 2011 Festo AG announced a radio-controlled ornithopter with bending wings. They are similar in function to the bending wings built by Erich von Holst in 1930s except that the wing twisting (not the bending action) is driven by a servo motor in each wing. This allows the amount of wing twist to be adjusted on the fly (Festo Corporate, 2012; The Ornithopter Zone, 2012).

2.2 Flight Types

There are two major flight types: flapping and fixed wing. Flapping wing flight is mostly used by natural flyers such as birds, insects, and fish and it is accomplished with a pair of wings ascending and descending with respect to their attachment points on the body. Flapping wing flight is very energy efficient and provides better maneuverability (Shyy *et al.*, 1999). However, the aerodynamics and kinematics of flapping wing flight are complex, and difficult to model and design. In comparison, fixed wing flight is very simple to model and build, but is rather crude with respect to maneuverability and energy inefficiency (Shyy *et al.*, 1999).

2.2.1 Flapping Wing Flight

Flight using flapping wings is natural to many creatures including birds and insects. Bird flight is more advanced and complex compared insect flight (Parslew *et al.*, 2010) while insect flight is considerably more repetitive. An insect moves its wings at higher frequency to generate lift and thrust. Due to high speed wing motion in insects, stroke angle and wing beat frequency remain mostly constant over time and no special flight characteristics are observed. In comparison, bird wing beat frequency is low and while birds are flying, they must continually adjust their wings during each stroke to remain airborne, change position, hover, land, or accelerate and decelerate. Thus, both the wing beat frequency and stroke angle continuously change in bird flight. Furthermore, birds use different forms of wing beats at different cruising speeds. In general, while they are flying, birds continually adjust their wings to generate a vertical force that is equal or greater to that of the gravity, and a horizontal force for forward

thrust. To be more precise and consider the role of feathers in flight, it is worthwhile to note that during take-off or slow speed flights, secondary bird feathers have no or little effect. At this time, during take-off, bird mostly requires lift and little or no thrust forces. Thrust and lift forces are mostly generated by primary feathers located on wings distal from the bird body. However, during normal or high speed flights, lift forces are generated by the inner part of the wing while tip feathers generate thrust forces during wing up and downstroke movements (Brown, 1948-1952; Shim *et al.*, 2007).

2.2.2 Fixed Wing Flight

Fixed wing flight is less complex compared to flapping wing flight. In fixed wing flight, the wing remain stationary and do not oscillate. Lift force generation is dependent upon wing shape and fluid passing by the wing surfaces. Most aerodynamic forces and moments that affect flight using fixed wings are due to the pressure and shear stress distribution over the body surfaces. Pressure forces act normal to the flying surface while shear forces act tangential to them. Depending on wing shape, a net upward pressure force can be generated to oppose the weight of the flying object and keep it airborne. This upward pressure force, referred as *lift*, is generated as long as the fluid is moving relative to the wing. In contrast, shear stresses generated by the same moving fluid generate frictional forces between the fluid and the flying surface, and hinder flight. The frictional forces generated by the passing fluid upon a surface are called *drag forces* (Anderson, 1984; Napolitano, 2012).

2.3 Bird Flight Biomechanics

Birds use various muscles, shown in Figure 1, while they fly to power the flight and to maneuver. The biomechanics of bird flight relates the muscles and feathers used during flight. Birds use various muscles and different feather groups during flight to power the flight and to maneuver. The following sections describe the various bird muscles and feathers, and their function.

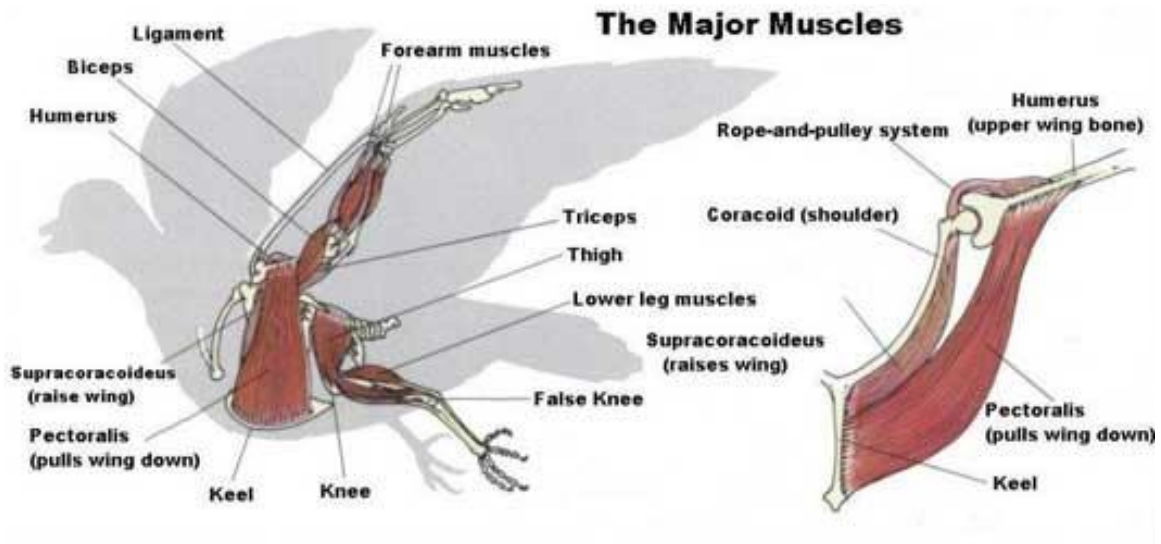


Figure 1: The muscle groups of a bird (Scott, 2012).

2.3.1 Muscles Involved in Bird Flight

The major muscles groups of a bird are shown in Figure 1. The pectoralis located at the chest of the bird is a Primary muscle that powers the wings for flight. The pectoralis is the largest muscle involved in flight and accounts for 8-11% of the body mass and about 60% of the total wing muscle mass. The major function of the pectoralis muscle is to lower and pronate wings at the shoulder during flight. The pectoralis provides enough power to keep the bird airborne and overcome drag forces during flight. This muscle contains relatively long muscle fibers which allow large muscular movement to be produced during muscle contraction and relaxation. The large muscular movement generates more power and accommodates large muscular strains during flight. In contrast, smaller muscles involved in flight deform a lot less, absorb less energy, and output lower power. While the wings are flapping, the pectoralis muscle is activated just before the wing reaches its top position during the upstroke. At this point, when the pectoralis muscle is activated, its muscle fibers are recruited and consequent force development takes place. The pectoralis muscle generates the maximum force shortly after the wing downstroke motion begins. Even though the pectoralis muscle is activated until the end of the downstroke, its deactivation process begins almost at the same time as it generates the maximum force, early during the downstroke. Thus, the deactivation process gradually decreases muscular force generation and slowly relaxes the muscle. By the time the wing downstroke is over, the force generated by the pectoralis muscle reaches zero, the muscle fibers completely relax, and the muscle prepares to stretch for the upstroke movement which is mostly powered by the the supracoracoideus muscle (Biewener, 2011; Tobalske, 2007).

The supracoracoideus muscle is about 5 times smaller in size than the pectoralis muscle and accounts for roughly 2% of the body mass. The supracoracoideus muscle is antagonist to the pectoralis, and is a primary wing elevator during the upstroke motion. The supracoracoideus is also involved in wing supination. The supracoracoideus is especially active during slow to moderate flight speeds and during hover, and not as active during high speed flights. It is believed that wing elevation during fast flights is partially caused by aerodynamic forces acting on the wing. These forces generated by the airflow assist the supracoracoideus muscle to raise the wing. The supracoracoideus muscle fibers are relatively short in length compared to that of the pectoralis. As a result, the supracoracoideus muscle does not generate much force during flight and is less accommodating to muscular strains. Similar to the activation time of the pectoralis muscle, the supracoracoideus muscle is activated towards the end of the wing downstroke motion, generates the maximum force early in the upstroke, and begins to relax shortly after the maximum force generation occurs (Biewener, 2011; Tobalske, 2007).

Other smaller muscles, such as biceps brachii, triceps brachii, metacarpi radialis, and carpi ulnaris, are also involved in bird flight. However, these muscles do not generate forces to support body weight or overcome drag. Instead, they help orient and control the wing during flight. These smaller muscles are responsible for maneuvering and efficient energy consumption by changing wing geometry to maximize the aerodynamics of flight. The smaller muscles have relatively short muscle fibers and long tendons which allows them to control distal parts of the wing while at the same time remaining small and lightweight (Biewener, 2011; Tobalske, 2007).

2.3.2 Feathers and Their Effect on Flight

Feathers are branched epidermal derivatives composed of matrix of intracellular keratin. Keratin is a structural protein produced by animals and it makes up animal hair, skin, feathers, or claws and nails. Feather consists of calamus, a rigid part of the feather that is inserted into the skin. Calamus is hollow and it continues with rachis, the central shaft of a feather. Each side of rachis is continued by set of filaments called barbs. Barbs have further extensions called barbules. Barbules from adjacent barbs overlap at 90°, and they are held together by hooklets. Hooklets are hook like projections on the barbules that maintain the shape of a feather, and they are responsible for strong connections that allow feathers to withstand aerodynamic forces that act upon wing during flight (Foster, n.d.; Prum, 1999).

Birds use primary feathers as their major means for generating lift and thrust during flight. Primary feathers are long and stiff and they can adjust to forces generated by fluid motion on the wing

such that they self-stagger in height and spread vortices both vertically and horizontally in the wake to reduce drag forces on the wing up to 25%. Furthermore, primary feathers are aligned in a manner that they generate pressure gradient across the wing when wings are flapping to cause an upward lift force production. More specifically, primary feathers can move with respect to each other and allow air passage in one direction, while in the other direction they will remain closely packed and air impermeable. During downstroke wing motion, primary feathers remain tightly held against each other to prevent air flow through the wing while they displace maximum amount of fluid to generate upward lifting force. In contrast, during wing upstroke, primary feathers separate in both horizontal and vertical directions and allow air passage in between. This separation of feathers during upstroke helps achieve a pressure gradient across the wing to produce an upward lifting force that keeps bird airborne. In comparison to primary feathers, secondary feathers are shorter in length and wider. These feathers do not generate any thrust, rather they help produce lift forces during flight (Eder *et al.*, 2011; Tucker, 1993).

2.3.3 Dynamics of Wing Motion during Flight

With birds, the upstroke wing kinematics and aerodynamics continuously vary with flight speeds while the downstroke kinematics is rather consistent across different flight speeds. Furthermore, wing motion kinematics also varies across species depending on wing shape. As expected, muscle activity also vary along with wing kinematics across different flight speeds. It has been shown that the wing upstroke motion is aerodynamically active during slow and medium speed flights. In general, during bird flight, as the flight speed of a bird increases, distal wing angle relative to its body midline decreases and the body angle relative to horizontal plane also decreases (Tobalske, 2003, 2007).

Slow Speed Flight

Birds usually enter slow speed flight during take-off or landing. During slow speed flight, the wings of the bird are positioned close to vertical to maximize generated lift forces. During takeoff, birds initially power their flight with thrust produced by their hind limbs (feet) followed by supporting wing flapping. The wing downstroke motion in slow speed flight begins when the wing is in an upward vertical position. During the downstroke motion, the wing is fully extended and moves downward until it is located slightly below the horizontal line across its connection with the body. This movement is due to the pectoralis muscle. At the end of the downstroke, the wing is swung forward and the moment manus (hand structure) of the wing is retracted facing the wing tips forward. Following the forward swing of the wing, the wing undergoes a movement that interchanges the downward motion into an upward one. The

upstroke motion starts when the previously flexed wing moves backwards and upwards while it gradually extends in preparation of a new cycle. Upstroke is finished when the wing reaches its original topmost position and is fully extended. During the upstroke, the wing is flexed at the elbow and the wrist to decrease negative lift force production. First, adduction of the humerus occurs. Next, the humerus is rotated along its long axis so that the radius and ulna nearly become vertical. Lastly, the wrist is further flexed and supinated. At this point, the wing is folded and rotated such that it moves backwards and upwards. The wrist is rotated to align the primary feathers in a vertical direction while the wing is lifted up. This movement at wrist is due to the biceps and the flexor carpi ulnaris muscles. In slow speed flights, the upward force is mostly generated during the wing downstroke and very little or no forward force is generated during the downstroke. The forward force is produced towards the end of downstroke when the wing is swung forward. The thrust force reaches its maximum value when wing undergoes the upstroke motion (Brown, 1948).

Medium Speed Flight

At medium speed flight, the wing movement is different from that in low speed flights. Starting from the downstroke, the wings are fully extended to about 50° above the horizontal. The wings then begin a downward and slightly forward motion to form a 90° arc. Once the downstroke is over, the upstroke begins with wings by slightly flexing at elbow. As the radius and ulna rise, the wrist of the bird is flexed and the manus is supinated. While the wing is moving upwards, the elbow and wrist are extended, and the hand is pronated to return back to the original fully extended shape. Similar to slow speed flights, the thrust forces in medium speed flights are produced by the primary feathers due to variations in the angle of attack of the moving fluid on a wing. The angle of attack changes during the upstroke motion when the wing is moving backwards and upwards (Brown, 1953)

Fast Speed Flight

The wing movement during fast flight is much different from both slow and medium speed flights. Wings during downstroke have only slight forward movement and upstroke has no propulsive backward flick while the wing is moving up relatively slowly. During the upstroke, the inner part of the wing is only slightly flexed and the wing is moving backwards and upwards. Once the upstroke is over, the wing is extended and moves slightly forward and downward. The thrust forces during fast speed flight are only produced by the wing tips during the downstroke. The downstroke becomes nearly vertical with smaller amplitude while it develops a greater forward thrust component from the wingtips. To be more

precise, wings during the downstroke simultaneously generate both lift and propulsive forces; the inner part of the wing produces the lift while the tips of the wing provide thrust (Brown, 1952).

2.4 Aerodynamics of Flapping Wing Flight

The aerodynamics of bird flight is rather complex compared to that of fixed wing flight. The complexity of flapping wing flight is due to birds altering their wing beat frequency, wing angle of attack, and stroke amplitude throughout the flight. Often, these alterations are applied to a single wing independently of the other and they make flapping wing aerodynamics even more intricate. Usually, the aerodynamics of bird flight changes according to flight type. For example, for soaring flight, the wings of the bird are fixed at one point, remain rigid and undergo similar aerodynamics to that of the fixed wing flight. However, when birds heavily rely on wing flapping for flight, their flight aerodynamics is very intricate and lead to unsteady flight. Despite its complexity, flapping wing aerodynamics provide birds with high maneuverability, an ability to fly at very low speeds, and high power and high aerodynamic efficiencies (Hedenström, 2002; Ho *et al.*, 2003; Linton, 2007; Von Ellenrieder *et al.*, 2008).

For any type of flight, whether it is achieved via fixed or flapping wings, the lift and drag forces are very crucial. The lift and drag forces generated during flight determine flight energy efficiency, flight speed, and maneuverability of a flying body. In general, the drag forces are generated when air is flowing parallel to the surface of an object that is traveling through the fluid. This type of drag force is called parasitic drag force and is associated with energy loss due to friction and relative motion that occurs between the fluid and the object surface. When air is flowing parallel to the surface of a wing, no lift force is generated. Another type of drag force is called a *form* drag force. Form drag force is generated during the wing downstroke and upstroke when moving fluid interacts with wing perpendicularly. Form drag force is responsible for lift generation while the wings undergo the downstroke motion and, to some degree, is also important in thrust generation as well. When the fluid is passing parallel to the wing surface, if a leading edge of the wing is rather inclined towards the moving fluid at a certain angle of attack, then, force applied to the wing by the air has two components: one directed vertically producing the lift force and the other directed horizontally. The assessment of the lift and drag forces in flapping wing flight is difficult since the large amplitude motion, and periodic acceleration and deceleration of the wings produce large inertial forces and unsteady effects that significantly deviate from standard linear aerodynamic and aeroelastic theories. Flapping wing aerodynamics is further complicated by wing deformation that is due to either intentional bending or varying wing material elasticity. Hence, steady

state aerodynamics does not accurately predict the aerodynamic forces generated during wing motion (Hedenström, 2002; Ho *et al.*, 2003; Linton, 2007; Popovic, 2013; Von Ellenrieder *et al.*, 2008).

It is necessary to note that the aerodynamic forces on the wing are due to the impulse of the wake momentum change when flapping wings deform the surrounding fluid. Wake momentum change is associated with the consequent formation and shedding process of the generated vortices. The shedding process of a vortex is in turn affected by the wing beat frequency and influences propulsive efficiency of the flight. The fact that flapping wings operate at low Reynolds number (10^3 to 10^6) where slight changes in the airflow can result in inhibition or promotion of wake separation signifies that airflow may change from turbulent to non-turbulent flow and vice versa and affect wing aerodynamics significantly. A high lift characteristic of flapping wing flight is due to the generation of an unsteady vortex bubble that is produced by flow separation of the sharp leading edge on the wings. This vortex is assessed in 3 dimensions and is spiral shaped. The three dimensional span wise flow of the air during the flapping directs the vortex from the leading edge towards the wing tip vortex and prevents the vortex on the leading edge of the wing to grow large and breakdown; this reduces the lift forces. Production of the vortex bubble and corresponding lift force generation begins during the first half of the downstroke when the axial motion of the spiral vortex forms a low pressure region on the upper part of the wing and causes it to grow as the wing downstroke continues. As the downstroke proceeds, another leading edge vortex forms that moves from the wingtips to the base of the wing. When the wing is supinated to transform the downstroke motion into the upstroke, these two vortices join to form a single vortex and shed from the trailing edge of the wing. During the upstroke, airflow over the wing is smooth on both surfaces allowing easy shedding of the vortex and minimizes the negative lift force production. Towards the end of the upstroke, a new vortex starts to grow from the underside of the wing causing negative lift forces. However, the negative lift generation during the upstroke is maximally limited due to several factors such as the primary feather alignment on the wings, partial folding of the wings during the upstroke, and reduction of the wingtip vertical speed during the upstroke. While the wing pronates to switch from the upstroke to the downstroke motion, the vortex produced during the upstroke rolls towards the leading edge and sheds. In this manner, about 80% of the lift forces are generated during the downstroke and the remaining lift forces are produced during the upstroke. Furthermore, during both upstroke and downstroke motions, the forces acting on the wings have forward components which account for the thrust during wing flaps. (Hedenström, 2002; Ho *et al.*, 2003; Linton, 2007).

Another important characteristic of bird flight is the Strouhal Number. A bird's efficient cruising locomotion requires the Strouhal number to be in the range of 0.2 to 0.4. Most birds use adaptive feedback to control of their wings to maximize their flight performance by manipulating and optimizing various unsteady and 3D flow mechanisms. Accordingly, birds adjust their wing beat amplitude and beat frequency to maintain a constant Strouhal number over varying range of flight speeds. For example, the Strouhal number during cruising flight is almost always 0.2. When the Strouhal number is 0.2, if bird wing is treated as a solid and non-elastic, the Strouhal angle will be 22° during the downstroke and -22° during the upstroke. The Strouhal angle corresponds to the angle of attack. However, the wing stalls at any angle larger than 15° , but stalling in flapping wing flight is prevented by the rotation of bird's wing about the shoulder which causes the angle of attack to vary from zero at the shoulder to the max value of 22° at the wingtip. As a result, the average angle of attack across the wing is below 15° and stalling does not occur (Ho *et al.*, 2003; Linton, 2007; Von Ellenrieder *et al.*, 2008).

A bird's tail also effects overall flight aerodynamics. At low speeds, the tail acts like a splitter plate and lowers parasitic drag up to 25%. The tail is also involved in additional lift production by preventing flow separation and is important for flight stability and control (Hedenström, 2002; Ho *et al.*, 2003).

Other aspects that are involved in flapping wing flight aerodynamics are Wing Loading and Wing Elasticity. Wing loading is a ratio of the weight of flying object to the wing area and describes the actions of gravitational and inertial forces against aerodynamic forces which are responsible for the lift and thrust generation. Higher wing loading allows flying objects to carry heavier masses but limits a bird's maneuverability, agility, and energy efficiency. Wing stiffness is involved in wing shape deformation which affects vortex generation during flapping which influences lift and thrust production. In general, the leading edges of bird wings are rigid. The rigidity of the wing edge helps produce an unsteady leading edge vortex. Maximum lift and thrust forces are generated with stiffer wing edges. On the other hand, the stiffer the wing body, the less thrust and lift are generated during flapping. In contrast to the wing edges, the wing regions that are located inward are more flexible. Inner wing flexibility mostly affects thrust production; more thrust is produced with elastic inner wings. Variable wing stiffness allows birds to precisely control the angle of attack on the wing by passive deformation of feathers and by manipulating shoulder, elbow, and wrist muscles. This, in turn, allows precise control of the vortex and wing interaction and it is important for both thrust and lift production (Ho *et al.*, 2003; Von Ellenrieder *et al.*, 2008).

Chapter 3: Project Strategy

3.1 Initial Client Statement

Before the start of the project, information on flapping wing flight was gathered and studied through literature search and patent review. Communicating with our client Professor Marko Popovic, an initial client statement was established as follows:

“To design and build a model that can successfully fly with flapping wings and has excellent aerodynamic qualities. This model should then be built to a larger scale for transportation of passengers. It can be maneuvered to deal with harsh environments during flight.”

The client statement states that the project aim is to build a model that can mimic a bird’s natural flight. However, this was thought to be too general and the original client’s statement needed more specificity. From the client’s statement, it was not clear what type of flapping flight should be mimicked. If the client desired to simulate a bird’s flapping wings, then, there is more specificity necessary as wing dynamics and kinematics during flight differs from species to species. In addition, the original client statement did not clearly state which aerodynamic qualities did the client want to optimize and which to neglect. Safety of flight was somewhat overlooked as well, and it had to be considered in more detail along with the dimensions of the design.

3.2 Revised Client Statement

After literature review and team discussions, many aspects of the initial client statement were found to be impossible to complete within the given budget of \$730 and time frame of 9 months. A compromise was made to partially satisfy the needs of the client and to make the project feasible. The revised client statement is as follows:

“Design and build a prototype that will be used to test flapping wing flight aerodynamics. More specifically, this design should enable researchers to experimentally generate and assess lift forces during flapping wing flight and compare them with theoretically derived values. This design should enable researchers to observe effects of wing area, flapping frequency, and the angle of wing rotation on lift force generation. The constructed prototype does not have to fly as long as it allows scientist to properly observe and understand characteristics of flapping wing flight. Similar criterion applies to design optimization; the design perfection isn’t of much importance as long as machine is able to flap its wings so that further understanding of the flapping wing mechanics is possible. This model will serve as a

precursor and testing model for a larger design which will be built later on as the project progresses. The larger model will be designed to carry cargo or even a passenger.”

The revised client statement states that goal of this project is to make a prototype to mimic wing flapping during flight. This model will serve to understand, compare, and test the basic aerodynamics involved during flapping wing flight. Model will help to compare and contrast experimentally and theoretically derived relationships between the forces involved during the flight, and different flapping wing characteristics such as wing area, flapping frequency, and wing angle of rotation.

The project will be carried out as follows. First, a small-scale, proof-of-concept prototype will be built for a feasibility study. The small-scale prototype will be followed by a larger, full-scale model that will assist researchers in understanding the aerodynamics of the flapping wing flight. The information that will be gathered from this project will be used to construct an improved and optimized model that mimics birdlike flight.

3.3 Objectives

All the objectives of this project point toward successful models that will be able to perform wing flapping and simulate flapping wing flight aerodynamics. If this objective is achieved, then researchers will be able to compare theoretical and experimental results and better understand the physics involved in flapping wing flight. Before reaching this goal of simulating flapping wing flight and observing its physical characteristics, certain milestones must be reached. Figure 2 shows an objectives tree that breaks down the main goal of this project into three branches.

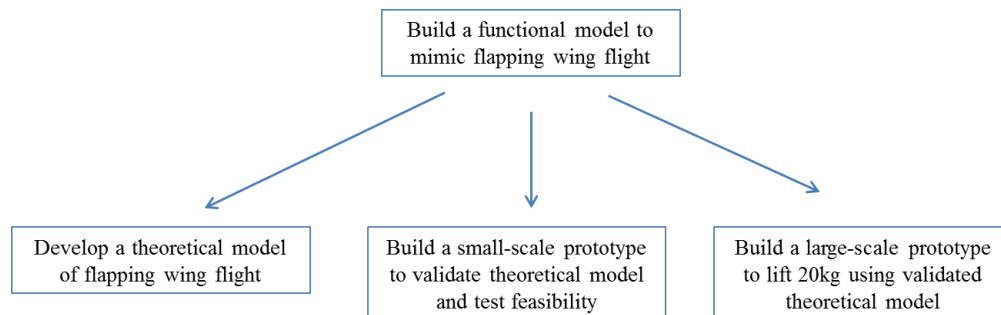


Figure 2: The Objectives Tree created to organize the project

First, a theoretical model of the aerodynamic forces involved in flapping wing flight will be developed. The theoretical model will be used to predict the lift force, flapping frequency, and power requirements for birdlike flight and determined design specifications. Next, a small scale proof-of-concept

prototype will be built and tested to validate the theoretical model. If the theoretical model is incorrect, the model parameters will be adjusted. With a validated theoretical model, a large-scale prototype will be designed. The theoretical model will be used to determine the necessary structural parameters of the large-scale prototype to lift 20 kg. Lastly, multiple experiments will be conducted with the large-scale prototype. A final report of the project will be provided to the client including recommendations for further enhancements to the prototype.

3.3.1 Cost

The built device and all the purchases associated with the project should not exceed the budget of the team. Team was given \$320 from Mechanical Engineering Department, \$160 from Biomedical Engineering Department, and \$250 from Physics Department. So the team has total of \$730 to spend.

3.3.2 Durability

The components of the device must withstand forces and moments while the device is being operated. The device must be fully functional throughout the experiment and should not break down. The device must be able to tolerate the cyclic motion of flapping wings over multiple cycles and repeated tests.

3.3.3 Safety

The device must be safe to operate. The device should not generate dangerous and harmful projectiles should the device fail during operation

3.3.4 Weight

Although achieving flapping flight is not an objective of this project, it is preferable to see the machine take-off, hence the device should be as light as possible. In addition, the lighter the weight, the more chances there are to detect and measure lift forces acting upon machine.

3.3.5 Manufacturability

The device should be easily manufactured. The device should limit the usage of custom made or hard to manufacture components. All of the components should be manufacturable at the WPI manufacturing shops.

3.3.6 Effectiveness

The design should be effective to satisfy the project goals and should effectively simulate flapping wing flight and produce aerodynamic forces that are similar to those observed during bird flight. The device must generate sufficient aerodynamic forces capable of being quantitatively described, recorded, and observed.

3.3.7 Easy to Operate

The device should be easy to operate without the need of complex computerized systems or special protective gear.

3.3.8 Pairwise Comparison Chart

A pairwise comparison chart, given in Table 1, was created to weigh the project objectives. This chart was filled out by both the team members and clients. According to the pairwise comparison chart, the safety of the device scored highest (4.5 out of 6.0). While lightweight and easy to build, objectives were scored lowest (1.5 out of 6.0). Accordingly, the safety of operator and observers was the most important factor during the design process, while weight and manufacturability objectives were less significant.

Table 1: Pairwise Comparison Chart. Notice that Safety scored highest while lightweight and easy to build scored lowest

Goals of the Design Process	Cost	Durability	Safety	Lightweight	Easy to build	Effective	Easy to Operate	Total Score
Cost		0	0	2	2	1	2	7
Durable	2		2	2	2	0	0	7
Safety	2	1		2	0	2	2	9
Lightweight	0	0	0		2	1	0	3
Easy to Build	0	0	2	0		0	1	3
Effective	1	2	0	1	2		1	7
Easy to Operate	0	2	0	2	1	1		6

3.3.9 Constraints

The constraints of this project can be identified as the factors that limit the team from achieving its objectives. Some of these constraints include time limit and the total budget. Other constraints associated with this project are limited access to more expensive and higher-quality materials such as titanium, carbon fiber, or higher quality aluminum alloys.. These materials are ideal for this project but are not attainable within the realm of the project budget. The amount of goals able to be accomplished is further limited by other graduation required classes that students have to take while they work on the project and availability of machining personnel and machines. Lack of time also poses threat to design quality as well because certain design specifications cannot be looked at in detail, nor can they be improved to perfection. Instead, team members have to work rapidly and use the parts of the machine that are rather simple and that will allow a proper functioning of the whole unit.

The size of the model represents another challenge to be overcome; it is rather difficult to machine and test large scale ornithopter. Due to a larger final size, the aerodynamic qualities of the flapping wings will significantly change. As a result of these changes, the device will require more power to flap its wings, which in turn will require stronger materials such as steel to be used. These materials will further increase the weight of the device.

3.4 Project Approach

To avoid wasting of resources, building the physical model will be conceptualized first using computer software and next on a small scale simpler design. To successfully perform these simulations, team will need to have equations that correctly formulate the aerodynamics involved in the flight of each design. Using these equations, the team will derive aerodynamic forces that are involved during flight and adjust design specifications in accordance to these calculations. Once the design parameters are set and verified by simulations, team members will acquire materials needed, machine them, and build the smaller device. After building and testing the first prototype, the team will re-adjust design parameters and build a second, more complex machine. The team will use both built devices to experimentally derive values of aerodynamic forces involved in flapping wing flight. As the dimensions of this model is an issue due to the change in aerodynamic qualities with increased device size, design parameters will be calculated in detailed manner and adjusted such that larger model will accommodate available motor.

The design will be made of mainly two components which are the wings and the body. Body will include most of the power transmission systems incorporating gears and shafts while the wings will provide surface area to displace enough air while they flap and produce lift. The biggest objective is to make the model safe for the user. The device will be designed for safety and it will sufficiently be tested to identify any possibility for failure. In this case, the design failure can be defined as model explosion and breaking of individual components. The model will be powered with a motor that will provide sufficient power output as demanded by calculations. During the experiment, the power outage from the motor will be adjusted below its maximum value to ensure that the model is safe. The wings will move with one degree of freedom; wings will flap up and down, forward and backward motion of the wings as described in natural bird flight will not be present. However, problem with one actuated degree of freedom flapping is that it is not very realistic, and even tiny asymmetry between left and right wing flapping will cause the bird to go into unstable state (Pfeiffer *et al.*, 2010).

Several meetings took place where both students and professors worked together to formulate equations that would correctly predict aerodynamic forces generated during flapping wing flight and quantitatively determine the forces that would cause the device to take off or fly. Firstly, the drag forces generated during flapping flight was assumed to act as the lift force and cause vertical takeoff during flight. This is true because birds generate drag forces in vertical direction while they flap wings and the direction of these forces act against gravity in vertical plane. Thus the lift comes from flapping wings, and forces are directed either upwards or downwards when birds continuously flap their wings. These forces then act upon wings and cause bird to lift off and fly. However, as mentioned in chapter two of this text, the wing flapping dynamics of the bird are adjusted such that negative lift force production is minimized during upstroke and majority of forces that are generated during flapping are directed upwards. While considering the lift force required for the model to takeoff, it was stated that this lift force must be greater than the model's weight. Prior to revising client's statement, team contemplated to build a 100 kg (980 N) flying device capable of lifting and transporting a human being. To achieve the max lift force for given weight, wing parameters that would give the optimized surface area were calculated using formula that incorporated wing surface area, forces produced during each flap, wing beat frequency, and power supplied from a motor (Appendix A). This shows that the wing length for optimal lift production is 2.25 m while the width is 2.00 m. Appendix A, presents equations that were used to derive lift force and other design parameters such as wing surface area, wing beat frequency, and power requirements of the wing flapping.

As the purpose of the smaller scale proof-of-concept model was to ascertain accuracy of the equations presented in Appendix A, these formulas were not taken into consideration for design optimization purposes during its design process. Rather, these equations were used to theoretically predict aerodynamic forces with given prototype parameters and compare them to the experimentally derived values. The first prototype was built out of 0.75 inch thick cast acrylic plate, 1/8 inch diameter plain steel rods, Duct Tape, and paper cards. These materials were processed and put together using laser cutter, bend saw, drilling machine, and tungsten arc welder in Washburn shops at Worcester Polytechnic Institute. The final structure of this prototype was put together using epoxy glue, bolts, screws, and washers. Shoulder bolts were used at joints where parts of the device had to move with respect to the body of the machine. Figure 3 shows the final structure of the first prototype. This device uses a gear system and a slider to transform rotational motion derived from the motor into up and down flapping motion. When the motor rotates, shaft on the gear causes the slider to move up and down which is connected with wings via two other shafts and makes wings to move up and down at 30° angle. According to the design parameters, wing movement had to be symmetric, producing a 15° angle of rotation below and above horizontal line. This model serves its purpose by being a simple mechanism able to continuously perform flapping motion.

Even though this design generated lift forces, they were not detected. As calculated, the lift forces generated with 50 cm by 30 cm wings, at the given flapping frequency were small in magnitude. These lift forces were on the order of 10 N. Unfortunately, the force plate upon which the device rested was not precise enough to correctly detect the force variation between wing upstroke and downstroke motions. As a result, experimental values could not be matched to those that were theoretically derived.

The final step of this project was to build a larger scale model based on our knowledge from the previous design and optimize the magnitude of produced lift forces such that measurement devices that were available to the team would detect them. To achieve this objective of producing a capable machine that would allow researchers to observe aerodynamics of the flapping wing flight, a pairwise comparison chart was constructed and objectives were evaluated therein. As shown in Table 1, many factors such as: cost, durability, safety, weight, easy to build, effectiveness, and easy to operate were taken into account. Each of these factors contributes to the success of the larger model design. These objectives were compared to each other and evaluated quantitatively. Higher score on the chart indicated relative importance of an objective with respect to the other goals.

Chapter 4: Design and Analysis

This chapter discusses the project needs, functions and goals, design process, the steps taken toward the realization of the physical prototypes, and experimental setups.

4.1 Needs Analysis

Originally, the goal of this project was to build an ornithopter capable of carrying an adult human and all the original equations were formulated and adjusted for that capability. However, while revising clients' statement, the goals of the project focused on building smaller scale testing devices. As a result, all previously calculated equations were used for characterization of aerodynamics despite downsized design parameters. Hence, the formulas are presented as they were originally devised and calculated.

4.2 Power Analysis: Flapping Wing and Fixed Wing Flight

Consider a bird-like mechanism with a pair of flapping wings, each with length $L=3m$ and width $W=2m$. Assume a drag induced hover or vertical takeoff (zero forward speed) resulting from wing flaps with constant angular speed ω between angles θ_0 during upstroke and $-\theta_0$ during the downstroke. For an angle θ , the required lift force for a zero vertical velocity hover is given by the following equation:

$$F(\theta) = 2 \int_0^L \cos\theta \frac{1}{2} \rho (\omega x)^2 C_d W dx = \cos\theta \rho \omega^2 C_d W \frac{L^3}{3}.$$

Given a drag coefficient of $C_d \cong 2$ and air density of $\rho \cong \frac{5kg}{m^3}$, the lift force is then

$$F(\theta) \cong \frac{5kg}{6m^3} WL^3 \omega^2 \cos\theta = 45 kgm \omega^2 \cos\theta.$$

Using the small angle approximation, $\cos\theta \cong 1$, the force is given by $F \cong 45kgm \omega^2$. Therefore, to lift a 100 kg, the bird-like mechanism requires $\omega \geq \sqrt{\frac{mg}{45kgm}} = 4.7 rad/s$. If $\theta_0 = \pi/12$, it would take approximately 0.11 seconds to complete the downstroke. The torque that the wing has to exert during the downstroke is given by the following equation:

$$\tau = \int_0^L \frac{1}{2} \rho (\omega x)^2 C_d W x dx = \rho \omega^2 C_d W \frac{L^4}{8} \cong 1.1 kNm$$

which corresponds to an independent wing power output of $\tau\omega = 5.2kW \approx 6.9hp$.

Typical Vespa engines are rated up to 100hp and the energy demanding takeoff phase may take only couple of seconds. After takeoff, the system can then enter a less energy demanding glide phase

accompanied with less frequent flapping. Hence, intelligent flying may prove to be energy efficient as well as a rapid means of transportation

Both static wing planes and helicopters utilize a lift generating pressure difference proportional to the difference in speed squared above and below the airfoil. For an airfoil with a simplified triangular shape (width W , height H , and length L), the lift force balancing weight implies the *lift induced drag* (via pressure difference) is equal to $mg\frac{H}{W}$. The total wing drag is approximated with the sum of *form drag* and *lift induced drag* given by $F_{drag} = \frac{1}{2}\rho(\omega x)^2 C'_d \rho v_{\parallel}^2 (2HW) + mg\frac{H}{W}$ where v_{\parallel} is forward speed. The *lift induced drag* dominates for small speeds and *form drag* dominates for large speeds of static wing and rotor blade with respect to air. The minimal power that the aircraft engine needs to produce to maintain a large enough forward velocity and stay in the air is obtained from the requirement that $F_{thrust} \geq F_{drag}$, i.e. $P_{min} = \left[\frac{1}{2}\rho(\omega x)^2 C'_d \rho v_{\parallel}^2 (2HW) + mg\frac{H}{W} \right] v_{\parallel}$. Furthermore, from the Bernoulli equation, $\frac{\rho v_{\perp}^2}{2} = \Delta p = \frac{mg}{2LW}$, thus $v_{\parallel} = v_{\perp} \frac{W}{H} = \sqrt{\frac{mgW}{\rho LH^2}}$ where v_{\perp} is air vertical speed. Therefore, the minimum required power is $P_{min} = \sqrt{\frac{m^3 g^3}{\rho LW}} \left(\frac{C_d W^3}{LH^2} + 1 \right)$. Utilizing the equation $\rho \cong \frac{5}{4} kg/m^3$, where $L=3m$, $W=2m$ and $m=100kg$, results in $P_{min} > \sqrt{\frac{m^3 g^3}{\rho LW}} = 11.2kW \approx 15hp$. Therefore, the most energy demanding condition for flapping wing aircraft (vertical takeoff) requires less power than the least energy demanding condition for static wing aircraft. This suggests that an actuated wing aircraft demands less energy than a static wing aircraft.

4.3 Functions and goals

The functions and the goals of the design are as follows. The model must be able to generate enough lift force to enable researchers to characterize the aerodynamics of the model and validate the equations. According to the goals of the project, two prototype models will be constructed: one used for proving of concept for feasibility study and the other model will be the final design that will meet the goals and perform the needed functions. The first prototype will be small-scale and used as a feasibility study and to validate the theoretical models. The first prototype will utilize rapid prototype techniques to decrease manufacturing time to allow for multiple design iterations. The large-scale design, on the other hand, will be more complicated and require more manufacturing time. The large-scale prototype will be larger than the first prototype and be constructed using more expensive and durable materials.

The overlying goal for this project is to pioneer a design process of building a human carrying ornithopter. Construction of a manned and flightworthy flapping wing vehicle is not necessary at this stage. Rather, the main function of the designs will consist of their ability to characterize aerodynamics of flapping wing flight and to identify and solve as many prevalent mechanical and engineering obstacles as possible. The devices built during the timeline of this project will ensure safety of the design team and operators during testing and they will be used as a basis for the future teams working on the same topic.

4.4 Conceptual Designs and their Specifications

To optimize a design for the client, it is important to have more than one proposed prototype. Multiple design choices offer more selectivity while multiple design iterations allow optimization and it encourages creativity so that the team can consider various approaches to the right solution. In addition, if one of the designs does not work or if the client dislikes the selected design, other designs could serve as substitutes. Ultimately, the major goal is to optimize the final design so that it is compliant to the specifications set by the client.

During the design process, the two prototypes were created, the first design being a small 2 kg prototype and the second one being a heavier 20 kg, biologically inspired ornithopters. These prototypes are incapable of self-sustaining flight, but they serve as examples of actuation mechanisms and can be used to explore various wing shape designs, to characterize various flapping strategies and sensory motor control, and to study the aerodynamics of flapping flight. More specifically, the first prototype validates the theoretical model and allows for feasibility testing, while the second prototype provides a platform for further testing.

4.5 Analytical Theoretical Flapping Flight Model

Theoretical model was developed first during the design process. The derived theoretical model can be found in appendix A and appendix B of this text.

4.6 Small-Scale Prototype Design

The first prototype design of the biologically inspired robot bird is shown in Figure 3. It is 1.2 in length from one wing tip to the other and 2 kg in weight. This design prototype can attain a 2.5 Hz flapping frequency. The body skeleton is assembled from laser cut acrylic pieces. The power transmission system consists of gears, a slider, and shafts. A primary gear that is connected to the motor spins at

constant speed and turns a secondary gear that is twice the size. The 2:1 gear ratio doubles the torque. The secondary gear is connected to a slider crank mechanism that drives the wing structure that is connected to wings. The wings ($L=0.6\text{m}$, $W=0.3\text{m}$) are made from metal wire and covered with duct tape and paper. More benefits of the crankshaft mechanism design include the compact packaging and the gears, slider crank mechanism, and wings are all attached to a single structural plate and they do not require additional machined parts or difficult assembly.



Figure 3: The fully assembled small-scale prototype design

4.6.1 Design and Manufacturing

Prototype for proof of concept testing was designed and built at 1:6 scale its full CAD design is shown in Figure 4. Prototype was made using 0.75 inch thick cast acrylic plastic. Plastic sheet was cut into pieces using laser cutter and Autocad software. Cut pieces of plastic were assembled together using bolts and various types of adhesives. For simplicity, wings were shaped after a rectangle and their lengths and widths were decreased by $2/3$. Skeleton of the wing was constructed from $1/8$ inch diameter stainless steel rod and $1/16$ inch aluminum angle bar. Stainless steel rods were welded together to form wing skeleton using an arc welding machine and aluminum rods were welded together similarly to make a hollow rectangular shape. Aluminum rectangle was attached to stainless steel skeleton using J.B. Welder glue and it was left to cure for 24 hours. Aluminum rectangles were then fit onto the acrylic ornithopter device and two holes were placed through each aluminum rectangular shape and acrylic rectangular bar. Once the holes were ready, screws were inserted in the holes and they were tightened using bolts. When the wing skeleton was finished, wing was covered using Duct Tape and paper Notecards. Duct tape was stretched across the wing width and wrapped around twice for each line. Notecards were inserted between the two Duct Tape lines about one inch deep along the width of the wing. Notecards were used to create

valves that open at one side (downward) when the wing was moving. There were total of three notecard lines inserted into the wing about 2.5 inches apart from each other.

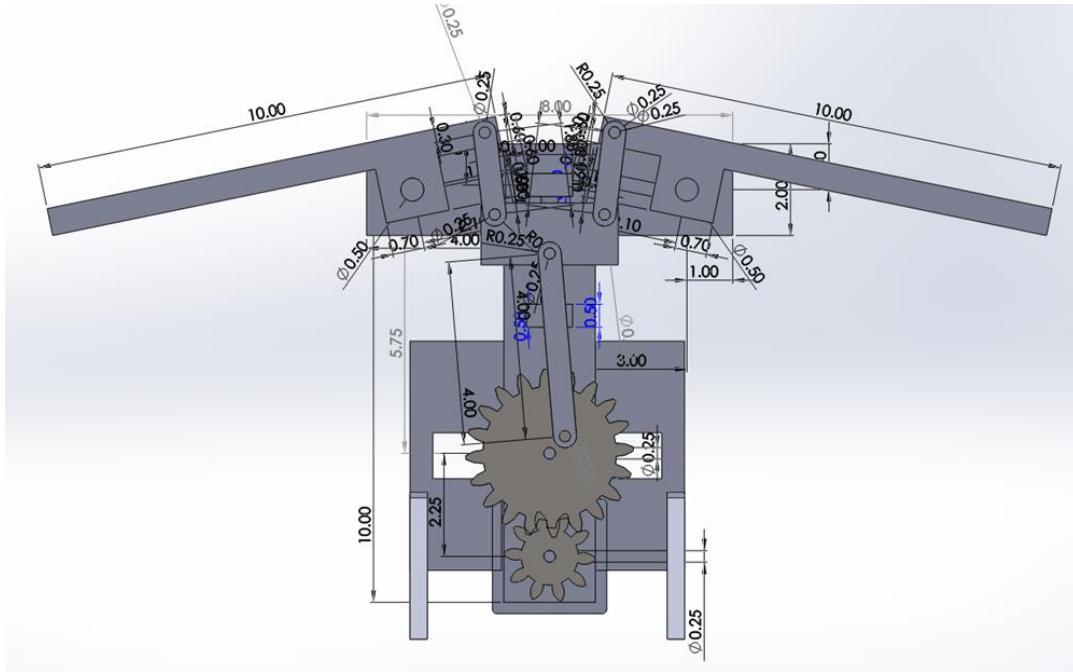


Figure 4: CAD drawing of the small-scale prototype design

4.6.2 Wing Design

In the design of the smaller prototype, basic rectangular shaped wings were designed using principles of flight observed in nature. To maximize lift production, the feathers on a bird's wing separate during the upstroke to allow free air passage while they remain tightly fixed to each other and air impermeable during the downstroke. This phenomenon was used in the first model wing design. Each wing in this model included three sets of flaps that passively opened during upstroke and allowed free passage of air through wings and closed during downstroke, cutting off air flow as shown in Figure 5. This mechanism displaces more fluid during downstroke and it causes generation of lift force. In contrast, the second model did not use the same principle for wing design. Rather, downstroke motion is faster than the upstroke resulting in more fluid displacement as air does not have enough time to flow past the fast moving wings. This wing design generates net upward lift force due to differences in wing upstroke and downstroke motion (Biewener, 2011).

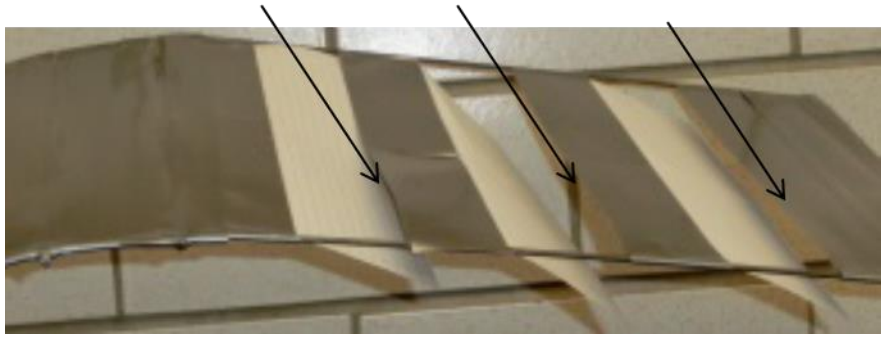


Figure 5: The valve mechanism for flapping wings. The valves passively open and close during wing motion.

4.6.3 Drive Mechanism

A crank-slider mechanism was used as the main drive mechanism of the small-scale prototype. Figure 6 shows the cranks slider mechanism attached to the wing structures. As the crank turned, the slider would be drive linearly up and down relative to the structure, driving connector rods attached to the wing structures.

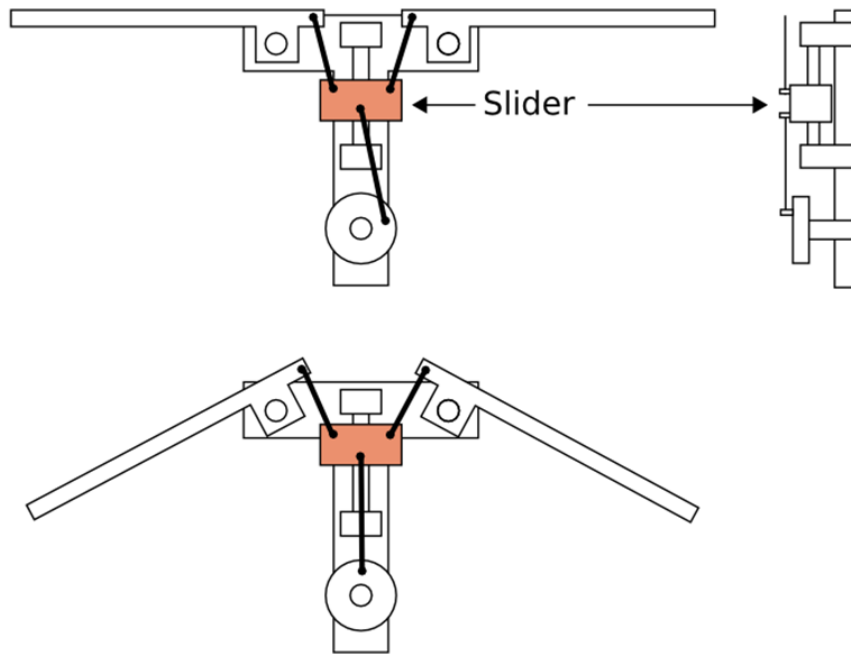


Figure 6: Diagram of the first prototype transmission system and wings

4.6.4 Experiment

Experiment for the small-scale prototype design was conducted as follows: force plate was set up and connected to computer. Sonar distance measurer was set up such that the displacement of the wing tip was measured. Data from both sonar distance measurer and force plate were analyzed and displayed using Logger Pro 3.8.6 software. High-speed camera was focused on one of the wings and film was taken at 240 frames per second for 5 to 10 seconds. Following filming, pictures of moving wing were taken at 30 frames per second. The device was attached on a platform so that no vibrations or movements were possible upon wing flapping. Motor was mounted on a platform and connected to the ornithopter prototype. The device and platform were then placed on the force plate on a leveled vertical position and the weight of the device was scaled to zero in the software. Motor was connected to the power source, and it was turned on at the highest power possible and data acquisition was begun.

Experiment was first conducted when the valves were opening downward during the wing upstroke and closing during the wing downstroke. Afterwards, wings were removed and adjusted in an upside-down position where valves opened upward during the wing downstroke. Next, data was recorded when valves were fixed motionless, so that they would not open and close upon the wing movement. Then, half of the wing covering was removed and machine was operated thus while flaps were motionless. Finally, during the last part of the experiment, data was collected when all the covering was removed from the wings and only the wing skeleton remained.

4.6.5 Small-Scale Prototype Design Summary

Given the motor specification (24V, brushed electric motor), this model is able to attain 2.5 Hz flapping frequency which results in negligible lift forces due to downward inertial forces from the wings and slider. Moreover, the model suffers from added complexities due to insufficiencies in design. Use of a slider crank drive mechanism provided many inherent disadvantages. One of the disadvantages with crank drive mechanism included wing motion. During flight, the wings spent more time above the horizontal rather than below it. Other disadvantages included wing rotation with non-constant angular speed due to the gear crank system when transforming upstroke movement into downstroke, movement and the transmission of forces at the worst transmission ratios, i.e. the crank would provide zero force at the initial descent of the downstroke. For these reasons, data from the first experiment was insufficient and the available force plate was not sensitive enough to detect generated lift forces. As a result new concepts were incorporated to build a second, larger model. This model would be more advanced in terms of

design aspects and it would generate more pronounced lift forces that could then be experimentally studied.

In addition to these problems during the experimentation, other technical issues also showed up. Namely, acrylic platform broke, and it had to be fixed using bolts. Furthermore, due to inertial forces, wings bent while they were flapping and they had to be straightened after experiment was over.

4.7 Large-Scale Model Design

The large-scale prototype, shown in Figure 7a, was designed using information and experience from the first smaller device. The second design was larger, did not include flaps on the wings, and did not have a slider crank drive mechanism. Rather, this design used paddle whackers and gears for force transmission and spring recoil for wing downstroke generation.

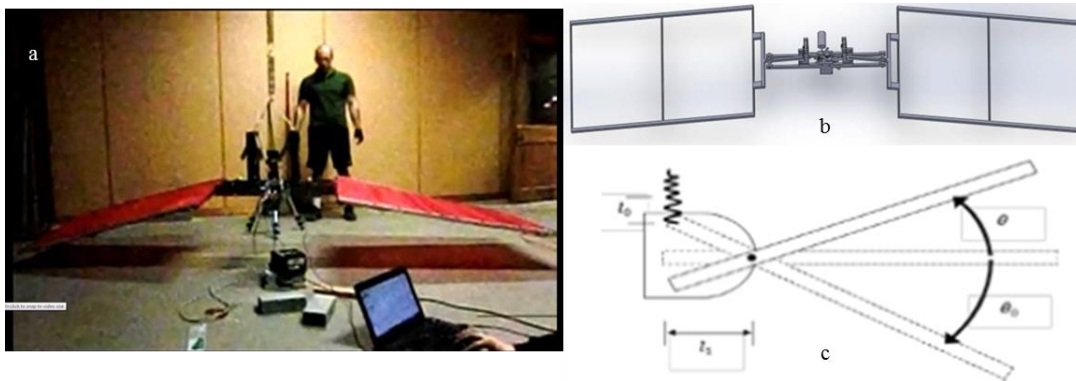


Figure 7: The design of the large-scale prototype: a) the experimental setup; b) A CAD model of the large-scale prototype; c) the wing motion trajectory of the large-scale prototype.

The second prototype has a 3.2 m wing span, weighs 22 kg and can attain a 4.0 Hz flapping frequency. The body skeleton was assembled from machined steel pieces. There is one gear per wing. Each gear carries four linear extensions or “paddles” that pushes the wings through the upstroke 4 times per gear revolution. The inner end of the wing structure is attached to a spring which hangs from the steel frame, when the wing moves through the upstroke, the spring stretches. When the motor is disengaged from wing the spring retracts quickly resulting in the rapid downstroke motion. A CAD model of the complete prototype is shown in Figure 7b. The wing motion is shown in Figure 7c. The wings ($L=1.22\text{m}$, $W=0.78\text{m}$) are made from aluminum alloy covered with rip-stop nylon

4.7.1 Manufacturing

Two smaller gears for the large-scale prototype design were produced from one big gear using CNC lathe machine. The big gear that was originally 3.40'' in length and 2.00'' in diameter was cut in half and processed to final shape. Shafts for the device were cut from 0.5'' diameter low carbon steel rod to desirable length of 4''. Next, 0.5 in length end segments of the cut shafts were reduced in diameter to 7/16'' using CNC lathe. After lathing, the shafts were threaded using a 7/16''-14 dye. The structure of the machine was made from low carbon 1/4'' thick 2'' or 3'' in wide steel bars. These bars were reduced to their final shape using CNC milling machine. Wing bones were made out of 1/2'' thick, 2'' wide low carbon plates, these parts too were processed using CNC mill. The flappers were made from 3/4'' thick 3'' by 3'' aluminum plates and 1/2'' diameter rods using CNC mill, manual threader, and manual taper. Once raw stock materials were machined, different parts were put together using either Tungsten Inert Gas (TIG) welding or Metal Inert Gas (MIG) welding machines. Wings were manufactured from 1/8'' thick 1'' by 0.5'' L-shaped aluminum rods and parachute nylon fabric. L-shaped aluminum rods were put together into wing frame using TIG welder while nylon was attached to the wings using high temperature hot glue gun and glue sticks. Once all the parts were manufactured, they were assembled together. Bearings were press fitted into plates and wing bones, and shafts were press fitted through the inner bearing holes. Wing bones were drilled and wings were attached to them using screws. Springs were placed on upper shafts and they were attached to the wing bones using chords. Motor was mounted on the aluminum plate, attached to the device via two 3/4'' diameter standoff rods, and connected to the driving shaft via spider coupler.

4.7.2 Drive Mechanism

This wing drive mechanism is a version of the One-To-Many (OTM) principle (Hunt *et al.*, 2012, 2013). The motor never directly engages the wing during lift generating downstroke. The spring-based drive mechanism in the larger ornithopter required the use of two cantilevered drive shafts in-between parallel plates. Slight misalignment between the plates caused either by manufacturing imprecision or by large force wing dynamics generated relative motion between the gears that engage wing bases. From the experiments, the misalignment varied a lot. Three situations were encountered during the experiments: large friction between gears, large friction between the gears and the wing bases, and gears barely touching each other and not engaging. This problem was solved by using gears that had relatively less and longer teeth. New gear teeth did not slide past one another and they remained fully engaged during the

experiment. The main advantage of the spring-based drive mechanism is that the motor never directly engages the wing during the lift generating downstroke. Instead, the motor slowly builds up energy in a wing elastic element during the slow upstroke. Hence, the power output can be multiple times larger than the power input. Similarly, there is no need for the motor to passively hold the wing since the wing elastic element is already in pre-tensed condition while the wing is at its lowest angular displacement and supported by a stopper. Since the motor is disengaged from wing during the powerful downstroke, no unexpected (motor damaging) drag induced torque may be encountered. Finally, due to pre-known conditions (i.e. wing spring constant and elongation), the motor may always rotate in same direction at a torque and velocity optimum to its performance curves.

4.7.3 Simulation

A detailed numerical dynamic simulator based on the heavy-weight (20 kg, $L=1.22\text{m}$, $W=0.78\text{m}$) model was developed. It includes the masses, center of mass locations, and moments of inertia of all parts treated as rigid bodies (deformations due to motion were neglected) as well as a constant wing spring (“muscle/tendon complex”, $k_1=1470\text{N/m}$) and constant tether spring ($k_2=300\text{N/m}$). The wing equation of motion during the downstroke includes drag forces with quadratic dependence on velocity, spring forces, and inertia terms. The entire “bird” equation of motion includes the weight, spring force, and lift force as a component of drag force and inertia terms. In this tethered condition, it takes approximately 50 milliseconds for charged spring to return to its original shape. Displacement of the center of mass of the body of the whole bird at this time is 1.2 centimeters above its resting state. After 250 milliseconds, the center of the mass of bird rises about 7 centimeters.

The hovering, single flap, steady state solutions for a scaled up un-tethered model with $m=100\text{kg}$, $L=3\text{m}$, $W=2\text{m}$ and same opening wing angle were evaluated. Both the wing spring constant (k_1) and time (t) when the downstroke is triggered after the apex (zero vertical velocity) were optimized to best match position and velocity cyclic conditions within the parameter space of interest. Various steady solutions exist and an average hovering power of less than 5.6kW ($t=0.02\text{s}$, $k_1=11\text{kN/m}$, leading to $f = 8.6\text{Hz}$ flapping frequency) per wing can be achieved. The simulation takes into account both strokes as well as non-zero vertical velocity during single steady cycle. Finally, the addition of non-zero forward speed makes these power requirements substantially smaller.

4.7.4 Experiments

In the tethered ornithopter experiment, ornithopter was hung from ceiling using rope-spring complex. Weight of the ornithopter was exactly balanced with tether spring force. The wings were then charged such that angular wing displacement from horizontal orientation was 15 degrees. Subsequent motion of the ornithopter was then recorded with 240 frames per second high-speed camera. The springs on the robot were loaded and released to induce wing flapping. Lift forces generated by the flapping wings were characterized by the upward displacement of the system. The experimental setup of the large-scale prototype is shown in Figure 7a.

4.8 Design Summary

Even though the first prototype provided some raw data, the force measurements obtained by this data were erroneous due to a substantial noise-to-signal ratio and absence of proper testing equipment; the smaller ornithopter did not produce enough lift force for the force plate. In comparison, the preliminary data from large ornithopter was in good agreement with theoretical calculations. Following the preliminary testing of the large device, the model was further repaired, fine-tuned, and prepared for full scale experimentation.

Due to the technical reasons the preliminary data from the smaller ornithopter experiments were not able to accurately characterize the physical model and validate theoretical calculations while that from the larger model did meet expectations.

Chapter 5: Results and Discussion

This chapter provides the results from the experiments completed on the small-scale and large-scale prototypes and a detailed discussion on the outcome of the results and project.

5.1 Experiments: Performance and Results

The following sections provide the results from the small-scale and large-scale prototype experiments.

5.1.1 Small-Scale Prototype Experiments

The small scale prototype experiment is discussed in detail in section 4.6.4. Even though the experiment was performed properly, due to the absence of the proper testing equipment relevant data was not acquired. The small-scale prototype model was able to successfully flap the wings, but it did not produce large enough lift forces that could be detected and recorded.

5.1.2 Large-Scale Prototype Experiments

In the experiment the ornithopter was tethered to a spring and its weight was exactly balanced with tether spring force. The ornithopter to do single flap following through the motion the displacement of the whole system rising above its resting position can be measured. When performing the experiment, the initial motor couldn't automatically flap the wings due to the high strength of springs to power supply from motor ratio. To overcome this, flapping motion of wings was done manually with a rope tied to the bases of the wings and charged by a team member stomping down the rope then releasing to induce a full flapping cycle. Each cycle was repeated 15 times, data collected, and displacement of the center of mass of ornithopter was recorded with a 240 frames/sec high speed camera.

The analytical approach of the results (i.e. the time to completion of downstroke and upward displacement due to the lift forces) closely matched the experimental results. The time required for completion of a downstroke and for springs to return to their original position was approximately 50 ms which was 6% faster from the theoretical value of 53 ms. According to theoretical analysis, at 53 ms, the center of the mass of ornithopter was expected to lift 1.26 cm above its resting position. In the experiment the ornithopter center of mass rose approximately 1 cm above its resting position upon completion of downstroke. The experimental height was 26% lower than the theoretical height. Although the full flapping cycle took 250 ms both theoretically and experimentally, the rising displacement of ornithopter

from its resting position varied. According to the calculations, the ornithopter should have displaced by 8.34 cm but in the experiments it only lifted 7.00 cm. There was a 19% decrease in height in the experimental value.

The errors that made our results different from the simulations were largely due to the fact that the flapping was done manually with each individual performing the flap of one wing; therefore the timing of the two wings' downstroke was varied. When releasing to induce the downstroke an immediate release of energy was needed. Because the flap was done manually the friction between the feet of the operators releasing the ropes and the ropes themselves prevented simultaneous immediate release causing a unsymmetrical and less powerful downstroke. Another factor to take into consideration is the stopper inhibiting spring recoil, which results in a hindered and incomplete downstroke. Due to the absence of proper testing equipment, all results were based upon observation of the recorded footage of experiment, potentially resulting in inaccuracies.

Further experiments were conducted so that a motor continuously powered the flapping motion. To have this work, the gears were redesigned and replaced to make sure they engaged and the wings were strengthened due to structural failures from the first experiment. The set up was similar to the previous experiment except that the wings were actuated by the motor hooked up to a control interface on a computer. This updated experiment gave satisfactory results such that when the wings flapped, the entire ornithopter fluctuated in a vertical direction, proving that it could lift its own weight. There were still many problems with the hardware that caused each of the two wings to flap independently. This made the whole system tilt, which rendered gathering displacement data very difficult, but through this experiment the team was able to observe more efficient flapping while avoiding some of the previous problems, namely avoiding inertial effects from the mechanism that reduced the ability to quantify lift forces

5.2 Discussion

The objectives of the project were to establish a theoretical analysis of flapping flight then manufacture two models to prove the equations. Constraints in this project other than limited time include funding and inexperience in regards to numerical simulations and machining, which required aid from outer sources. Additionally, since there are no other projects described like this in available literature, the team couldn't compare results. For this reason, we created our own theoretical model and compared our

results to that model. Our theoretical model concluded that flapping flight requires less power than typical fixed-wing flight and this statement was validated by the second prototype.

5.2.1 Feasibility Study and Theoretical Model Validation

The small-scale prototype experiment was not able to provide any useful results and did not serve its purpose as a proof of concept. From this failure, many things design issues were established. The force plate was not suitable to measure the small lift forces generated by the small-scale prototype. A better solution would have been to create a force plate sensitive enough to read the small lift force. The inability to gain substantial data from the small-scale prototype was a major setback since it could not provide comparative information for the theoretical model.

5.2.2 Final Design Testing

Results from the large-scale prototype showed that the experiment was successful because the raw data was close to the data from the simulation. From this fact, the ornithopter ultimately did serve as a proof of the theoretical concept. This also meant that the power saving aspect of flapping flight is also a valid statement.

Furthermore, these conclusions have impacts in many areas such as economics, the environment, society, politically, manufacturability, and sustainability.

5.2.3 Economic Considerations

From an economic standpoint, a functioning full-scale ornithopter would have an immense change because there could potentially be a whole new kind of product available in the market as an alternate aircraft. Since the results tell us that there is less power necessary for the flapping flight, less fuel would be needed, saving money for the consumer. The extent of how this novelty would impact the economy would depend on the demand of the customers

5.2.4 Environmental Impact

Fuel efficiency has a very positive impact for the environment. This project may reduce the amount of pollution caused by the aircraft in addition, the proposed method of flying doesn't require large runways that conventional fixed-wing flying aircraft need. The space saved by reducing the size of airports means less destruction of the surrounding environment.

5.2.5 Societal Impacts

There are potentially many positive societal impacts from this project. Flapping wing flight has multiple advantages including being fuel-efficient, environmentally friendly, and the airfare may cost less. As a result, people may prefer this mode of flying. However, flight stability during flight may become an issue since the flapping of the wings may cause passengers to feel uneasy.

5.2.6 Political Impacts

Politically, such a product may give rise to a lot of attention in the global market. In order for this merchandise to enter the market, it would have to go through some examination under the law just as many novel inventions need approval from the Federal Aviation Administration (FAA). This examination would involve verifying the safety of the passengers and the ability of aircraft to fly as well as an investigation as to why it is superior to existing aircraft.

5.2.7 Manufacturability

Manufacturability of such model is hard to tell specially because we haven't produced a large enough robot that could potentially carry a passenger. The vehicle needs to be able to actuate the wings to flap for takeoff and landing but also to tilt the wings while staying fixed at a position for gliding. Reproducibility of such a model may be challenging for any company for it has never been built before especially in a large-scale.

5.2.8 Sustainability

Sustainability refers to how this proposed method of flying affects biology/ecology in terms of renewable energy. One of the special features of this product is that it requires less energy to function than the already existing fixed wing aircraft. This means that we would be able to use electric motors, which are too weak for the conventional aircraft, but powerful enough for our model.

Chapter 6: Conclusions and Recommendations

6.1 Conclusions

Although no fundamental obstacle exists for developing a human carrying ornithopter robots capable of hovering solely by flapping wings, none have been successfully built. This project tried to solve this issue by pioneering the steps for building such a device, and by proving that ornithopters are more advantageous over fixed wing and rotary blade aircraft through experimentation. To validate the claim, an analytical study, power analysis, and physical experiments were conducted towards the realization of an ornithopter robot capable of hovering and generating a 100 kg lift force. Then the results from the theoretical study were scaled down and experimentally tested. The analytical study and power analysis indicated that for a human carrying ornithopter, an average hovering power of 5.6 kW is achievable via a flapping wing mechanism which is less than the 11.2 kW needed for an equivalent fixed-wing aircraft. Two prototypes were constructed to validate the theoretical model of flapping flight and both models utilized two different actuation and control mechanisms. Multiple experiments were performed under repeatable lab conditions. The experiment with the final design was successful and it validated the proposed aerodynamic numerical model with reasonable accuracy. Ornithopters have many innate advantages over fixed-wing and rotary blade aircraft. Due to their high maneuverability, large range of possible speeds, and reduced power requirements, ornithopters may be a viable and attractive mean of intelligent transportation that deserves more dedicated research and practical realization.

6.2 Recommendations

In the future, teams working on the same project should address the following: motor power output, transmission system, and wing design. The motor should be powerful enough to displace the springs and release them in an appropriate manner. Instead of having one powerful motor, two smaller ones can be used; however, motor operation must be synchronized. The transmission system requires gears that have large enough teeth that correctly engage and do not slip with respect to each other while power is transmitted. The gears need to be adjusted such that both paddle whackers simultaneously engage the wing bones. Furthermore, the shaft that is connected to the gears in current design is cantilevered; this promotes undesirable lateral motion of the shafts. Depending on the size of gear teeth, the lateral motion either causes gear disengagement or unsynchronized wing flaps. Thus, the cantilevered shafts must be removed and a more rigid system designed and built. Finally, the wings should include valves that open

during the upstroke and close during the downstroke. The current wing design did not incorporate valves; as a result, during the experiment, the forces causing downward bird motion were produced in addition to lift forces.

References

- Anderson, J. D. (1984). *Fundamentals of aerodynamics*. New York: McGraw-Hill.
- Anderson, J. D. (2002). *The airplane: A history of its technology*. Reston, VA: American Institute of Aeronautics and Astronautics.
- Baek, S. S., Bermudez, F. L. G., & Fearing, R. S. (2011). Flight control for target seeking by 13 gram ornithopter. 2674-2681. doi: 10.1109/IROS.2011.6048246
- Barry, A. J., Jenks, T., Majumdar, A., & Tedrake, R. (2013). *Flying between obstacles with an autonomous knife-edge maneuver*. Under review MIT, 2013.
- BBC News - Film-maker Kaayk admits hoax over "bird-man suit" video. (2012). *BBC - Homepage*. Retrieved April 28, 2013, from <http://www.bbc.co.uk/news/world-europe-17487366>
- Biewener, A. A. (2011). Muscle function in avian flight: Achieving power and control. *Philosophical Transactions of the Royal Society of London. Series B, Biological Sciences*, 366(1570), 1496-1506. doi: 10.1098/rstb.2010.0353
- Brooks, A.N. , MacCready, P.B., Lissaman, P.B.S., & Morgan, W.R. (1985). Development of a Wing-Flapping Flying Replica of the Largest Pterosaur, AeroVironment Inc. AIAA/SAE/ASME/ASEE 21st Joint Propulsion Conference, July 1985 Monterey, CA. AIAA-85-1446
- Brown, R. H. J. (1948). The flight of birds; the flapping cycle of the pigeon. *The Journal of Experimental Biology*, 25(4), 322.
- Brown, R. H. J. (1952). The flight of birds II; wing function in relation to flight speed. *The Journal of Experimental Biology*, 30(1), 90-103.
- cyberneticzoo.com » Bourdon Tube Toys. (2012). *cyberneticzoo.com* . Retrieved April 28, 2013, from <http://cyberneticzoo.com/?tag=bourdon-tube-toys>
- Dashevsky, E. (2011). DARPA's robot hummingbird takes war on nectar to a new level: This little remote control robotic hummingbird can fly in any direction or even hover in place. while it looks like a souped-up fishing lure, small robots like this may just be the future of combat. *ExtremeTech.Com*
- DeLaurier, J. (1994). An Ornithopter Wing Design. *Canadian Aeronautics and Space Journal*, 40, 10-18.
- DeLaurier, J. D. (1993). An aerodynamic model for flapping-wing flight. *Aeronautical Journal*, 97(964), 125-130.
- DeLaurier, J. D. (1999) "The development and testing of a full-scale piloted ornithopter." *Canadian aeronautics and space journal* 45(2), 72-82.

- DeLaurier, J. D. (2005). Project Ornithopter. *Project Ornithopter*. Retrieved March 27, 2013, from <http://ornithopter.net>
- Deubel, T., Wanke, S., Weber, C., & Wedekind, F. (2007). Modelling and manufacturing of a dragonfly wing as basis for bionic research. *Strojarstvo*, 49(1), 25-30.
- Diaz, J. (2012). Man Flies Like a Bird Flapping His Own Wings. *Gizmodo, the Gadget Guide*. Retrieved April 28, 2013, from <http://gizmodo.com/5894904/man-flies-like-a-bird-flapping-his-own-wings>
- Eder, H., Fiedler, W., & Pascoe, X. (2011). Air-permeable hole-pattern and nose-droop control improve aerodynamic performance of primary feathers. *Journal of Comparative Physiology. A, Neuroethology, Sensory, Neural, and Behavioral Physiology*, 197(1), 109-117. doi: 10.1007/s00359-010-0592-7
- Ellington, C. (1991). Limitations on animal flight performance. *Journal of Experimental Biology*, 160, 71-91
- Festo Corporate (2012) “SmartBird – bird flight deciphered”, Retrieved July, 2012, from http://www.festo.com/cms/en_corp/11369_11468.htm#id_11468
- Foster., & Smith. (n.d.). Bird Feather Types, Anatomy, Molting, Growth, and Color. *Pet Health Care / Dog and Cat Behavior Information by Veterinarians*. Retrieved January 31, 2013, from <http://www.peteducation.com/article.cfm?c=15+1829&aid=2776>
- Hedenström, A., Department of Biology, Lund University, Naturvetenskap, Evolutionär Ekologi, Lunds universitet, (2002). Aerodynamics, evolution and ecology of avian flight. *Trends in Ecology & Evolution*, 17(9), 415-422. doi: 10.1016/S0169-5347(02)02568-5
- Hedenström, A., Department of Biology, Lund University, Naturvetenskap, Evolutionär Ekologi, Lunds universitet, . . . Science. (2002). Aerodynamics, evolution and ecology of avian flight. *Trends in Ecology & Evolution*, 17(9), 415-422. doi: 10.1016/S0169-5347(02)02568-5
- Ho, S., Ho, C., Nassef, H., Pornsinsirak, N., & Tai, Y. (2003). Unsteady aerodynamics and flow control for flapping wing flyers. *Progress in Aerospace Sciences*, 39(8), 635-681. doi: 10.1016/j.paerosci.2003.04.001
- Hunt, R., Hornby, G., & Lohn, J. (2005). Toward evolved flight. 957-964. doi: 10.1145/1068009.1068172
- Hunt, T. R., Berthelette, C. J., Iannacchione, G. S., Koehler, S., & Popovic, M.B. (2012) Soft Robotics Variable Stiffness Exo-Musculature, One-To-Many Concept, and Advanced Clutches. IEEE ICRA 2012 WORKSHOP: Variable Stiffness Actuators moving the Robots of Tomorrow, St. Paul, Minnesota, May 14 2012.

- Hunt, T. R., Berthelette, C. J., Popovic M. B. (2013) Linear One-to-Many (OTM) system: Many degrees of freedom independently actuated by one electric motor” accepted to the 5th Annual IEEE International Conference on Technologies for Practical Robot Applications (TePRA), Greater Boston Area, Massachusetts, USA, April 22-23, 2013
- Jackowski, Z.J. (2009). Design and construction of an autonomous ornithopter. MIT SB Thesis. Retrieved March 28, 2013, from <http://dspace.mit.edu/handle/1721.1/52809>.
- Kim, D., & Han, J. (2006). Smart flapping wing using macrofiber composite actuators. *Smart Structures and Materials*. International Society for Optics and Photonics, 2006
- Kim, D., Han, J., & Kwon, K. (2009). Wind tunnel tests for a flapping wing model with a changeable camber using macro-fiber composite actuators. *Smart Materials and Structures*, 18(2), 024008-024008 (8). doi: 10.1088/0964-1726/18/2/024008
- Lin, C., Hwu, C., & Young, W. (2006). The thrust and lift of an ornithopter's membrane wings with simple flapping motion. *Aerospace Science and Technology*, 10(2), 111-119. doi: 10.1016/j.ast.2005.10.003
- Linton, J. O. (2007). The physics of flight: II. flapping wings. *Physics Education*, 42(4), 358-364. doi: 10.1088/0031-9120/42/4/004
- Mazaheri, K., & Ebrahimi, A. (2010). Experimental investigation of the effect of chordwise flexibility on the aerodynamics of flapping wings in hovering flight. *Journal of Fluids and Structures*, 26(4), 544-558. doi: 10.1016/j.jfluidstructs.2010.03.004
- Mueller, T. J., American Institute of Aeronautics and Astronautics, & Ebrary Academic Complete. (2001). *Fixed and flapping wing aerodynamics for micro air vehicle applications*. Reston, Va: AIAA, Inc.
- Napolitano, M. R. (2012). *Aircraft dynamics: From modeling to simulation*. Hoboken, NJ: J. Wiley.
- Norton, R. L. (2011). *Machine design: An integrated approach*. Boston: Prentice Hall.
- Paranjape, A. A., Dorothy, M.R., Chung, S., & Lee, K.D. (2012) A Flight Mechanics-Centric Review of Bird-Scale Flapping Flight. *International Journal of Aeronautical and Space Sciences*, 13(3), 267-281.
- Parslew, B., & Crowther, W. J. (2010). Simulating avian wingbeat kinematics. *Journal of Biomechanics*, 43(16), 3191-3198. doi: 10.1016/j.jbiomech.2010.07.024

- Pfeiffer, A. T., Lee, J., Han, J., & Baier, H. (2010). Ornithopter flight simulation based on flexible multi-body dynamics. *Journal of Bionic Engineering*, 7(1), 102-111. doi: 10.1016/S1672-6529(09)60189-X.
- Popovic, M. (2013). *Biomechanics and Robotics*. Boca Raton: Pan Stanford Publishing (in press).
- Prum, R. O. (1999). Development and evolutionary origin of feathers. *Journal of Experimental Zoology*, 285(4), 291-306.
- Regan, W., Van Breugel, F., & Lipson, H. (2006). Towards evolvable hovering flight on a physical ornithopter. Computational Synthesis Lab, Cornell University, Ithaca NY
- Send, W., Fischer, M., Jebens, K., Mugrauer, R., Nagarathinam, A., & Scharstein, F. (2012). Artificial Hinged-Wing Bird with Active Torsion and Partially linear kinematics. 28th International Congress of the Aeronautical Sciences, Göttingen, Germany 2012
- Scott. "On Wings of Eagle." Polite Dissent - On Wings of Eagles. Polite Dissent, 25 Dec. 2012. Web. 29 Apr. 2013.
- Shim, Y., & Husbands, P. (2007). Feathered flyer: Integrating morphological computation and sensory reflexes into a physically simulated flapping-wing robot for robust flight manoeuvre. (pp. 756-765). Berlin, Heidelberg: Springer Berlin Heidelberg. doi: 10.1007/978-3-540-74913-4_7
- Shyy, W., Berg, M., & Ljungqvist, D. (1999). Flapping and flexible wings for biological and micro air vehicles. *Progress in Aerospace Sciences*, 35(5), 455-505. doi: 10.1016/S0376-0421(98)00016-5
- Singer, B., & Ebrary Academic Complete. (2003). *Like sex with gods: An unorthodox history of flying*. College Station: Texas A & M University Press
- Slaboch, P. (2002) Flying Like the Birds. *Flying Like the Birds*. Retrieved December 29, 2012, from www.nd.edu/~techrev/Archive/Winter2002.
- SmartBird - bird flight deciphered, Presented at TEDGlobal (2011) , Edinburgh, UK, July 11 - 15 , 2011. http://www.festo.com/cmslen_corp/11369.htm
- Sterchak, R. (2009). *Ornithopter having a wing structure and a mechanism for imparting realistic, bird-like motion thereto*
- Subbaraman, N. (2009). Robotic Bird Flies Over MIT | Scope. *Scope / The Publication of the Graduate Program in Science Writing at MIT*. Retrieved March 28, 2013, from <http://scopeweb.mit.edu/?p=671>
- The Ornithopter Zone (2012) Fly Like A Bird - Flapping Wing Flight, Retrieved July, 2012, from <http://www.ornithopter.org/>

- Tobalske, B. W. (2007). Biomechanics of Bird Flight. *The Journal of Experimental Biology*, 210, 3135-3146.
- Tobalske, B. W., Hedrick, T. L., & Biewener, A. A. (2003). Wing kinematics of avian flight across speeds. *Journal of Avian Biology*, 34(2), 177-184. doi: 10.1034/j.1600-048X.2003.03006.x
- Torenbeek, E., Wittenberg, H., & SpringerLink ebooks - Engineering. (2009). *Flight physics: Essentials of aeronautical disciplines and technology, with historical notes*. Dordrecht: Springer Netherlands. doi: 10.1007/978-1-4020-8664-9
- Tucker, V. (1993). Gliding birds - reduction of induced drag by wing tip slots between the primary feathers. *Journal of Experimental Biology*, 180, 285-310.
- Von Ellenrieder, K. D., Parker, K., & Soria, J. (2008). Fluid mechanics of flapping wings. *Experimental Thermal and Fluid Science*, 32(8), 1578-1589. doi: 10.1016/j.expthermflusci.2008.05.003

Appendix A: Detailed Calculations

A.1 More detailed calculation

$$\text{Drag Force: } F_d = \frac{1}{2} \rho v^2 C_d A$$

For a rectangular shaped wing which has length L and width W , with flapping angle of θ_0 at the constant angular speed of ω , total lift force:

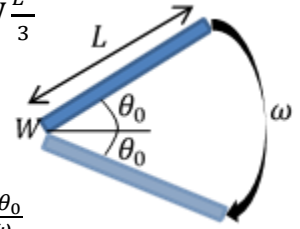
$$\begin{aligned} |F_v(\theta)| &= \cos(\theta) \int_0^L \frac{1}{2} \rho v^2 C_d dA = \cos(\theta) \int_0^L \left[\frac{1}{2} \rho (\omega r)^2 C_d W \right] dr \\ &= \cos(\theta) \frac{1}{2} \rho \omega^2 C_d W \frac{L^3}{3} \end{aligned}$$

$$\text{For 2 wings, } F_v(t) = 2 \cos(\theta_0 - \omega t) \frac{1}{2} \rho \omega^2 C_d W \frac{L^3}{3} = \cos(\theta_0 - \omega t) \rho \omega^2 C_d W \frac{L^3}{3}$$

$$\text{Period for downstroke: } \frac{T}{2} = \frac{2\theta_0}{\omega}$$

Average Force by 2 wings:

$$\begin{aligned} F_{v,ave} &= \frac{\int_0^{T/2} F_v(t) dt}{T/2} = \frac{\int_0^{\frac{2\theta_0}{\omega}} \frac{\rho C_d W L^3}{3} \omega^2 \cos(\theta_0 - \omega t) dt}{\frac{2\theta_0}{\omega}} = \frac{\rho C_d W L^3}{3} \omega^2 \int_0^{\frac{2\theta_0}{\omega}} \cos(\theta_0 - \omega t) dt \\ &= \frac{\rho C_d W L^3}{6\theta_0} \omega^3 \left[-\frac{1}{\omega} \sin(\theta_0 - \omega t) \right]_0^{\frac{2\theta_0}{\omega}} = \frac{\rho C_d W L^3}{6\theta_0} \omega^3 \left[-\frac{1}{\omega} \sin(\theta_0 - 2\theta_0) + \frac{1}{\omega} \sin(\theta_0) \right] \\ &= \frac{\rho C_d W L^3}{6\theta_0} \omega^3 \left[2 \frac{1}{\omega} \sin(\theta_0) \right] = \frac{\rho C_d W L^3}{3} \frac{\sin(\theta_0)}{\theta_0} \omega^2 \end{aligned}$$



$$\text{Torque for 2 wings: } \tau(\theta) = 2 \int_0^L |\vec{r} \times \vec{F}| d\vec{r} = 2 \int_0^L \left[r \frac{1}{2} \rho (\omega r)^2 C_d W \right] dr = \rho \omega^2 C_d W \frac{L^4}{4}$$

$$\text{Power: } P = \tau \omega = \rho \omega^3 C_d W \frac{L^4}{4}$$

$$\text{If } \theta_0 = 30^\circ, F_{v,ave} = \frac{\rho C_d W L^3}{\pi} \omega^2 \text{ and } \tau = \frac{\rho C_d W L^4}{4} \omega^2 \text{ and } P = \frac{\rho C_d W L^4}{4} \omega^3 \text{ for 2 wings.}$$

$$\text{For } \rho = 1.22 \text{ kg/m}^3, C_d = 2, W = 2 \text{ m}, L = 2 \text{ m}, \omega = 8.9 \frac{\text{rad}}{\text{s}} \text{ (} f = 4 \text{ Hz)}$$

$$F_{v,ave} = 981 \text{ N}, \tau = 1546.2 \text{ Nm}, P = 13760 \text{ W}$$

$$\text{For } \rho = 1.22 \text{ kg/m}^3, C_d = 2, W = 2 \text{ m}, L = 2 \text{ m}, \omega = \frac{4\pi}{3} \frac{\text{rad}}{\text{s}} \text{ (} f = 2 \text{ Hz)}$$

$$F_{v,ave} = 218 \text{ N}, \tau = 342.5 \text{ Nm}, P = 1434.6 \text{ W}$$

Appendix B: General Flapping Theory

Equation of motion for center of mass (CM) of entire bird with mass M , consisting of two wings each with mass m_W and body with mass m_B , is

$$F_{drag} - F = Ma_{CM} = M \frac{dv_{CM}}{dt}$$

where F_{drag} representing the wings' flapping induced drag forces and with constant force $F = Mg$ for vertical flying or $F = F_{friction}$ for horizontal swimming on ground surface (as discussed here). Here, positive axis points perpendicular above wings. Hence $v_{CM} > 0$ for vertical takeoff (or forward horizontal swimming) or $v_{CM} < 0$ for vertical landing (or backward horizontal swimming).

The CM momentum can be split into wings' CM and body's CM contributions as

$$2m_W v_W + m_B v_B = M v_{CM}$$

where all CM velocities in respect to air.

Wings' CM velocity, in small angle approximation, can be related to body's velocity as

$$v_W = v_B + l_{CM} \omega$$

where l_{CM} is the wing's CM distance from center of rotation, depending on wings geometry and mass distribution. Here, wing's angular velocity in respect to body, ω , is assumed positive for rotations from above to below body. Hence, from (2) and (3) body's CM velocity is

$$v_B = v_{CM} - \frac{2m_W}{M} l_{CM} \omega .$$

The drag force can be expressed as

$$F_{drag} = 2 \int_0^L \frac{1}{2} C_d \rho W (l\omega - v_B)^2 \text{sign}(l\omega - v_B) dl,$$

or

$$F_{drag} = \frac{1}{3} C_d \rho W \omega^2 \left[\left(L - \frac{v_B}{\omega} \right)^3 \pm \left(-\frac{v_B}{\omega} \right)^3 \right] \text{sign}(\omega),$$

with positive sign if $0 < \frac{v_B}{\omega} < L$, negative sign otherwise, and with $C_d \cong 2$ being drag coefficient, $\rho = 1.25 \text{ kg/m}^3$ air density at room temperature, W wing's width, and L wing's length.

Substituting v_B in terms of v_{CM} gives

$$F_{drag} = \frac{1}{3} C_d \rho W \omega^2 \left[\left(L + \frac{2m_W}{M} l_{CM} - \frac{v_{CM}}{\omega} \right)^3 \pm \left(\frac{2m_W}{M} l_{CM} - \frac{v_{CM}}{\omega} \right)^3 \right].$$

Substituting the drag force into the equation of motion gives the first order differential equation for v_{CM} in terms of ω . Here, angular velocity may be independent of v_{CM} or may depend on v_{CM} as we

discuss later on. As expected CM acceleration in respect to air, a_{CM} , is function of CM velocity in respect to air, v_{CM} , and wing's angular velocity in respect to body, ω .

B.1 Model Dependent Dynamics

Our flapping mechanism assumes three phases: charging, release and neutral. Charging phase is defined as period when motor engages spring and charges it with potential elastic energy (wing stroke from below to above body). Release phase is defined as period when spring is released from motor and freely engages wing (wing stroke from above to below body). Neutral phase is defined as period when wing is in contact with stopper and spring is in tensed state (wing is at rest in respect to body and positioned below body).

Neutral phase drag force (for $\omega_n = 0$) can be expressed as $F_{drag} = -C_d \rho W L v_{CM}^2$. Charging phase drag force (for $\omega_c < 0$) can be expressed as $F_{drag} = -\frac{1}{3} C_d \rho W \omega_c^2 \left[\left(L - \frac{v_B}{\omega_c} \right)^3 - \left(-\frac{v_B}{\omega_c} \right)^3 \right]$. Release phase drag force (for $\omega_r > 0$) can be expressed as

$$F_{drag} = \frac{1}{3} C_d \rho W \omega_r^2 \left[\left(L - \frac{v_B}{\omega_r} \right)^3 + \left(-\frac{v_B}{\omega_r} \right)^3 \right].$$

Charging phase angular velocity is assumed constant. Release phase angular velocity can be obtained as solution to wing equation of motion

$$\tau_{spring} + \tau_{drag} + \tau_{gravity} = I \alpha_r = I \frac{d\omega_r}{dt}$$

where I being wing moment of inertia and α_r release phase angular acceleration. Torque by spring

$$\tau_{spring} = k l_1 [(-\theta + \theta_0) l_1 + l_0]$$

is expressed in terms of lever arm l_1 corresponding to distance between spring attachment point and center of rotation, minimal elongation of spring l_0 , corresponding maximal angle θ_0 (assumed positive for wing below body), spring constant k , and instantaneous wing angle θ . Torque induced by drag is

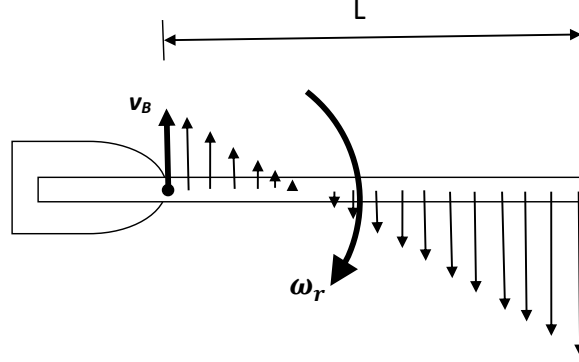
$$-\tau_{drag} = \int_0^L \frac{1}{2} C_d \rho W (l\omega - v_B)^2 \text{sign}(l\omega - v_B) l dl$$

or

$$-\tau_{drag} = \frac{v_B}{2\omega} F_{drag} + \frac{1}{8} C_d \rho W \omega_r^2 \left[\left(L - \frac{v_B}{\omega_r} \right)^4 + \left(-\frac{v_B}{\omega_r} \right)^4 \right].$$

The drag force and torque are coupled first order differential equations that can be numerically solved for v_{CM} and ω_r given appropriate boundary conditions.

Analytical solution exists for decoupled simplified cases with $v_B \cong 0$ and $I \cong 0$ given the initial and final angular velocities for release phase. Substituting the spring, drag, and gravity torques into the wing equation of motion and take the derivative leads to a constant and negative angular acceleration. Hence, angular velocity can be defined in time.



If $0 < \frac{v_B}{\omega} < L$, with $\omega_r > 0$, $v_B > 0$ as in Fig above, equation (5a) can be expressed as

$$F_{drag} = 2 \int_0^L \frac{1}{2} C_d \rho W (l\omega - v_B)^2 \text{sign}(l\omega - v_B) dl$$

$$= C_d \rho W \omega^2 \left[- \int_0^{v_B/\omega} \left(l - \frac{v_B}{\omega} \right)^2 dl + \int_{v_B/\omega}^L \left(l - \frac{v_B}{\omega} \right)^2 dl \right]$$

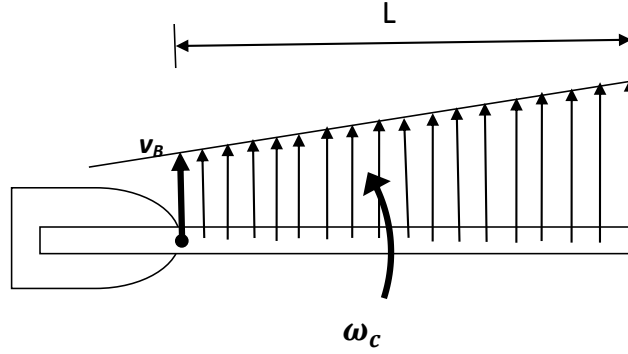
$$F_{drag} = C_d \rho W \omega^2 \left[-\frac{1}{3} \left(l - \frac{v_B}{\omega} \right)^3 \Big|_0^{v_B/\omega} + \frac{1}{3} \left(l - \frac{v_B}{\omega} \right)^3 \Big|_{v_B/\omega}^L \right] = C_d \rho W \omega^2 \left[-\frac{1}{3} \left(\frac{v_B}{\omega} \right)^3 + \frac{1}{3} \left(L - \frac{v_B}{\omega} \right)^3 \right]$$

Similarly, the drag torque can be expressed as

$$\begin{aligned} -\tau_{drag} &= \int_0^L \frac{1}{2} C_d \rho W (l\omega - v_B)^2 \text{sign}(l\omega - v_B) l dl \\ &= \int_0^L \frac{1}{2} C_d \rho W (l\omega - v_B)^2 \text{sign}(l\omega - v_B) \left[\left(l - \frac{v_B}{\omega} \right) + \frac{v_B}{\omega} \right] dl \\ &= \frac{1}{2} \frac{v_B}{\omega} F_{drag} + \frac{1}{2} C_d \rho W \omega^2 \int_0^L \left(l - \frac{v_B}{\omega} \right)^3 \text{sign}(l\omega - v_B) dl \end{aligned}$$

and hence the draft torque for $\tau_{drag} < 0$

$$-\tau_{drag} = \frac{1}{2} \frac{v_B}{\omega} F_{drag} + \frac{1}{8} C_d \rho W \omega^2 \left[\left(L - \frac{v_B}{\omega} \right)^4 + \left(\frac{v_B}{\omega} \right)^4 \right]$$

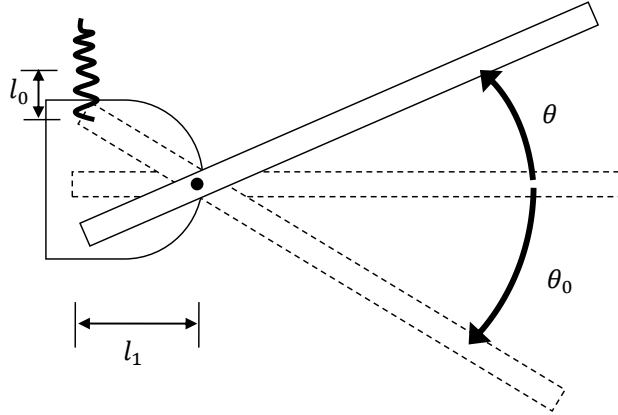


If $\frac{v_B}{\omega} < 0$, with $\omega_c < 0$, $v_B > 0$ as in Fig above, equation (5a) can be expressed as

$$F_{drag} = 2 \int_0^L \frac{1}{2} C_d \rho W (l\omega - v_B)^2 \text{sign}(l\omega - v_B) dl = C_d \rho W \omega^2 \left[- \int_0^L \left(l - \frac{v_B}{\omega} \right)^2 dl \right]$$

$$F_{drag} = -C_d \rho W \omega^2 \frac{1}{3} \left(l - \frac{v_B}{\omega} \right)^3 \Big|_0^L = -\frac{1}{3} C_d \rho W \omega^2 \left[\left(\frac{v_B}{\omega} \right)^3 + \left(L - \frac{v_B}{\omega} \right)^3 \right]$$

Here we ignore $\tau_{gravity}$ which is otherwise equal to $m_W g l_{CM}$.

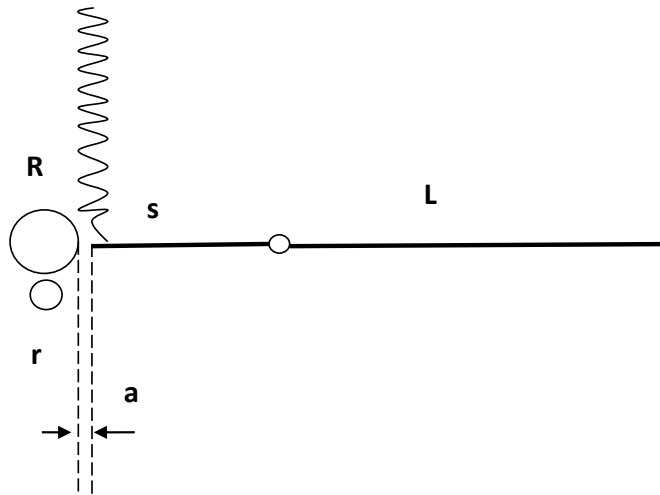


When spring engages wing for $-\theta_0 < \theta < \theta_0$ (in figure above angle is negative) spring torque equals

$$\tau_{spring} = k l_1 [(-\theta + \theta_0) l_1 + l_0]$$

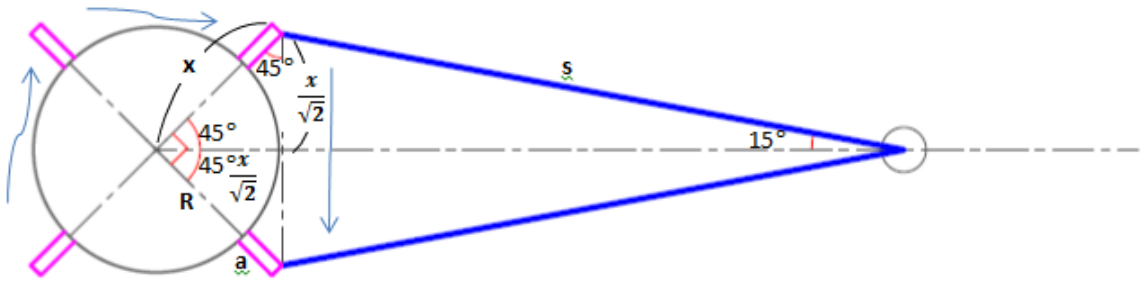
in a small angle approximation. This torque is positive.

B.2 Quick Estimation of Forces and Moments for the Second Prototype



1. Force from wing $\sim 50\text{N}$
2. Moment from wing is $< 50\text{N times } L$
3. This requires force from gear "R" onto "s" that is $< 50\text{N times } L/s$
4. This requires moment from gear "R" that is $< 50\text{N times } L/s \text{ times } (R+a)$
5. This requires force from motor gear "r" onto "R" that is $< 2 \text{ times } 50\text{N times } L/s \text{ times } (R+a)/R$
6. Finally this corresponds to required motor moment of $< 2 \text{ times } 50\text{N } (L/s)((R+a)/R)r$

For above numerical example and assuming $L=1.5\text{m}$ one obtains that $s=0.3\text{m}$ and max vertical extension of "s" from horizontal level and for 30 degree angle is $h=0.15\text{m}$. Hence, if spring attachment is very close to the edge of "s" the required spring force, according to 3) should be less than $50\text{N } (L/s)=250\text{N}$. Based on that one could estimate that spring constant, k , should be at least bigger than $F/h=1700\text{N/m}$.



$$\frac{x}{\sqrt{2}} = s * \sin \theta$$

$$x = R + a = \sqrt{2}s * \sin \theta$$

$$d(\text{spring displacement}) = \frac{2x}{\sqrt{2}} = 2s * \sin \theta$$

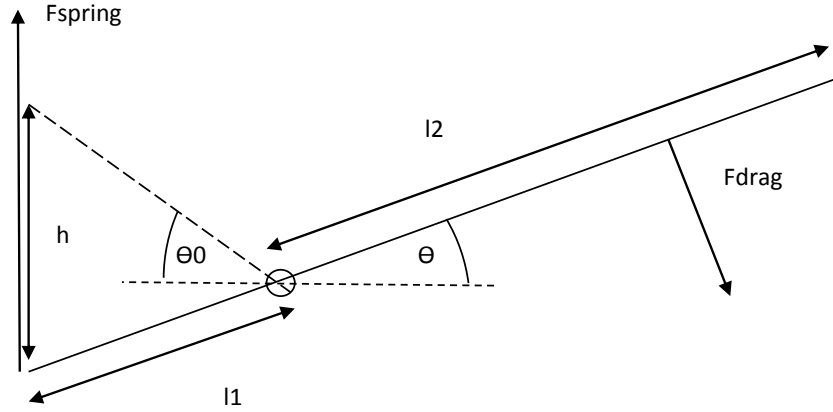
$$F(\text{force on spring}) = \frac{50L}{s} = K * d$$

$$K(\text{spring constant}) = \frac{50L}{sd} = \frac{50L}{2s^2 * \sin \theta}$$

Choose $s = 12in = 0.3048m$, $L = 1.2m$, $\theta = 15^\circ$.

Then $x = 4.39in = 0.111565m$, $d = 6.212in = 0.1578m$, $F = 197N$, $K = 1248N/m$

B.3 Calculation of Spring Engagement Duration



The Moment (i.e. torque) due to spring will be equal to moment due to drag. Here I am ignoring gravity.

Hence,

$$l_1 F_{spring} \cos(\theta) = \int_{0.1016}^{l_2+0.1016} \frac{1}{2} C_d \rho W (l\omega)^2 l dl$$

where

$$F_{spring} = k(l_1(\theta_0 + \theta) + 0.04)$$

therefore

$$k(l_1^2(\theta_0 + \theta) + 0.4l_1)\cos\theta = \frac{1}{2} C_d \rho W \frac{[(l_2 + 0.1016)^4 - 0.1016^4]}{4} \omega^2$$

$$\left(\frac{8k[l_1^2(\theta_0 + \theta) + 0.4l_1]\cos\theta}{C_d \rho W [(l_2 + 0.1016)^4 - 0.1016^4]} = \omega^2 \right)$$

and by taking derivative of both sides

$$kl_1^2[-\sin\theta(\theta_0 + \theta)\omega + \omega\cos\theta] - 0.04kl_1\omega\sin\theta = \frac{1}{2} C_d \rho W \frac{[(l_2 + 0.1016)^4 - 0.1016^4]}{4} 2\omega\alpha$$

Dividing both sides by ω

$$kl_1^2[-\sin\theta(\theta_0 + \theta) + \cos\theta] - 0.04kl_1\sin\theta = C_d \rho W \frac{[(l_2 + 0.1016)^4 - 0.1016^4]}{4} \alpha$$

where α is angular acceleration apparently constant and equal to

$$\alpha = \frac{4kl_1^2[-\sin\theta(\theta_0 + \theta) + \cos\theta] - 0.04kl_1\sin\theta}{[(l_2 + 0.1016)^4 - 0.1016^4]C_d\rho W}$$

Finally by using kinematics relation $2\theta_0 = \omega_0\Delta t + \frac{1}{2}\alpha(\Delta t)^2$ and $\omega = \omega_0 - \alpha\Delta t$, one can obtain that

$$\alpha(\Delta t)^2 + 2\omega_0\Delta t - 4\theta_0 = 0$$

$$\Delta t = \frac{-\omega_0 \pm \sqrt{\omega_0^2 + 4\alpha\theta_0}}{\alpha}$$

Appendix C: Source Code

D.1 Simulation Matlab Code

```
clear all;clc;close all
N=1; Q=N*250;
M=22; g=9.81; lcm=3*2.54/100; MI=0.04; c=2; rho=1.25; W=0.78; L=1.22; theta0=pi/12;
mw=1.5; mb=19; tt=0.001; l1=0.254; l0=0.087; k=1470;
Fd=zeros(1,Q);vcm=zeros(1,Q);vb=zeros(1,Q); theta=zeros(1,Q);
w=zeros(1,Q);Tdrag=zeros(1,Q);
vcm(1)=0; vb(1)=0; z(1)=0; i=1;
w(1)=0.0001; theta(1)=-theta0;
while theta(i)<theta0;
    if 0<vb(i)/w(i)<L & w(i)>0
        Fd(i)=(c*rho*W/3)*w(i).^2*((L-vb(i)/w(i)).^3-(vb(i)/w(i)).^3); 101 %sign(w)=1,
case+
    end
    if 0>vb(i)/w(i) & w(i)<0
        Fd(i)=-(c*rho*W/3)*w(i).^2*((L-vb(i)/w(i)).^3+(vb(i)/w(i)).^3); 102 %sign(w)=-
1, case-
    end
    if 0<vb(i)/w(i)<L & w(i)<0
        Fd(i)=-(c*rho*W/3)*w(i).^2*((L-vb(i)/w(i)).^3-(vb(i)/w(i)).^3);103 %sign(w)=-1,
case+
    end
    if 0>vb(i)/w(i) & w(i)>0
        Fd(i)=(c*rho*W/3)*w(i).^2*((L-vb(i)/w(i)).^3+(vb(i)/w(i)).^3);104 %sign(w)=1,
case-
    end
    if vb(i)>0
        Tdrag(i)=-(vb(i)*Fd(i)/(2*w(i)))+(c*rho*W/8)*w(i).^2*((L-
vb(i)/w(i)).^4+(vb(i)/w(i)).^4); 105 %when spring release, case+
    end
    if vb(i)<0
        Tdrag(i)=-(vb(i)*Fd(i)/(2*w(i)))+(c*rho*W/8)*w(i).^2*((L-vb(i)/w(i)).^4-
(vb(i)/w(i)).^4);106 %when spring release, case-
    end
    Tspring(i)=k*l1*((-theta(i)+theta0)*l1+l0);
    Tgravity=mw*g*lcm;
```

```

w(i+1)=w(i)+(Tspring(i)+Tdrag(i)+Tgravity)*tt/MI;
theta(i+1)=theta(i)+w(i)*tt+.5*(Tspring(i)+Tdrag(i)+Tgravity)*tt^2/MI;
Fspring=M*g-z(i)*300;
vcm(i+1)=vcm(i)+((Fd(i)+Fspring)/M-g)*tt;
vb(i+1)=vcm(i+1)+(2*mw/M)*lcm*w(i+1);
z(i+1)=z(i)+vb(i)*tt;
i=i+1;
end
while i<250

    vcm(i+1)=vcm(i)+((Fspring)/M-g)*tt;
    vb(i+1)=vcm(i+1);
    z(i+1)=z(i)+vb(i)*tt;
    i=i+1
end;
plot(z)
xlabel('time [ms]'); ylabel('height [m]');

```

Appendix D: Design Matrix

Means Feature/Function	1	2	3	4	5	6
Power supply	Electric Motor	Regular Gas Engine	Nitrous Engine			
Power Delivery/Storage System	Shaft Cylindrical (hollow)	Shaft Cylindrical (solid)	Rotational Spring	Regular Spring	Cable	
Bird Support	Circular shape	Vertical stand	4 bar support			
Bird Support materials	Steel	Aluminum	Wood	Plastic		
4 bar support shapes	Cylindrical (hollow)	Rectangular (hollow)	Cylindrical (solid)	Rectangular (solid)		
Shaft Material	Steel	Aluminum	Carbon Fiber			
Motor to Shaft, Shaft to Bird Connection	Universal joints					
Wing Power Delivery System Materials	Steel	Aluminum	Plastic			
Wing Skeleton	Rectangular rod (solid)	Cylindrical rod (solid)	Rectangular Rod (hollow)	Cylindrical rod (hollow)		
Wing Skeleton Material	Aluminum	Steel	Carbon Fiber			
Wing Covering Material	Nylon	Plastic	Paper/Cardboard			
Flaps on the Wing	Prof. Nestinger's Design	Prof. Popovic's Design	Bo Rim's Design	Nick's Design	Phil's Design	Woo Chan's Design
Flap Material	Paper	Nylon	Plastic	Nylon/Carbon Fiber		
Gears	Spur Gears	Worm Gears	Bevel gears	Miter Gears		
Gear Material	Steel	Aluminum	Plastic	Brass		
Bird Body Material	Steel	Aluminum	Plastic	Wood		
Bearings	Shoulder Bolts	Ball bearings (metallic)	Ball bearings (plastic)			

Appendix E: Analytical Stress Analysis

E.1 Stress Analysis for Prototype II Wings

The experiment conducted to gather preliminary data for the second design gave us valuable experimental results. Unfortunately, wings of the device broke towards the end of experiment after data was gathered. The following text includes analytical analysis to determine the fatigue of the wing materials.

In this Project, the wings were built using 90 degree angle aluminum edge bars. Due to the failure of the first wings, it is necessary to estimate stresses that wing is experiencing through each flap and how many cycles the wing can endure before the failure. The tensile strength of the aluminum, according to the vendor (McMaster-Carr) is $S_{UT} = 35kpsi$.

For the given tensile strength, the fatigue strength of the material can be estimated by using the following equation (Norton, 2011):

$$S'_f = 0.4S_{UT} = 14kpsi$$

This fatigue strength corresponds to 5×10^8 cycles in the S-N curve however this value needs to be corrected by the equation:

$$S_f = C_{load}C_{size}C_{surf}C_{temp}C_{reliab}S'_f$$

Assuming a *pure torsional* loading $C_{Load} = 1$. Since the cross section of the bar is a shape of an “L” equations 6.7b, 6.7c, 6.7d can be used from Norton’s book to figure out the C_{size} . Eventually, by using these equations, value of $C_{size} = 1$. Value for the machined finish C_{surf} was bigger than 1 so $C_{surf} = 1$. $C_{temp} = 1$ because the material is aluminum. For a 90% reliability, $C_{reliab} = 0.897$.

$$S_f = (1)(1)(1)(1)(.897)(14) = 12.558kpsi$$

In order to make an S-N diagram, estimated strength (S_m) of the material must be known. Hence, using equation 6.9 (Norton, 2011):

$$S_m = 0.9S_{UT} = 31.5kpsi$$

To predict the number of flaps the wing can endure before failure, alternating stress (σ_a) must be found by using the equations below:

$$A_{tot}c_1 = A_1a_1 + A_2a_2 \quad (E.1)$$

$$I_n = \frac{bh^3}{12} \quad (E.2)$$

$$I_{tot} = [I_1 + A_1(c_1 - a_1)^2] + \dots [I_n + A_n(c_1 - a_n)^2] \quad (E.3)$$

$$\sigma_a = \frac{Mc_2}{I_{tot}} \quad (E.4)$$

$$\sigma_b = \frac{Mc_1}{I_{tot}} \quad (E.5)$$

where A_{tot} is the total area of the cross section of the bar, and A_1 and A_2 are areas of each designated sections of the cross section. The rest of the variables represent dimensions as shown in in the Figure E.1.

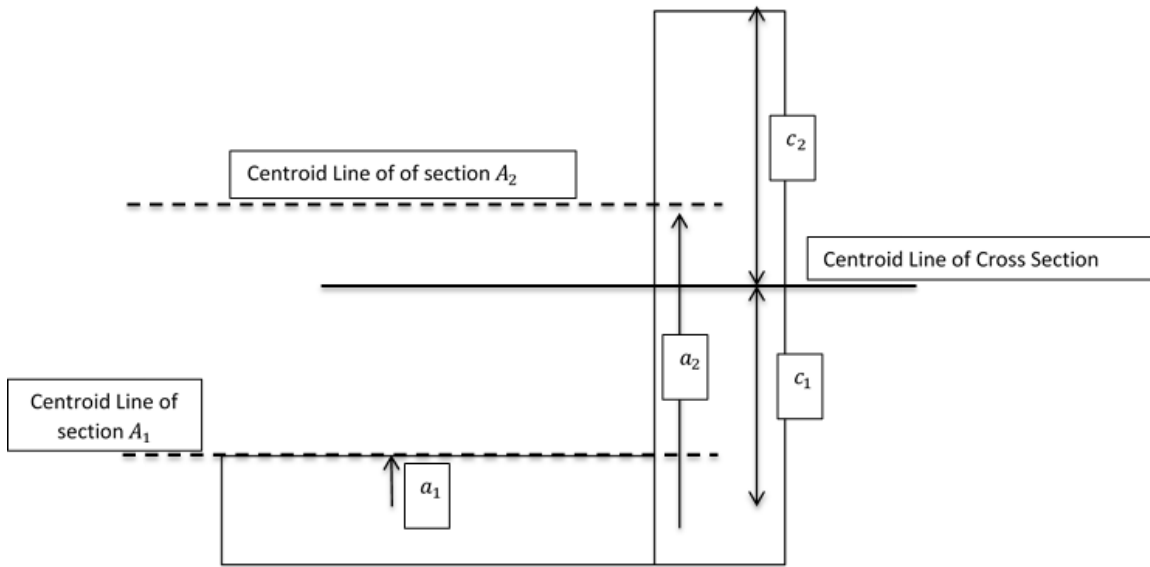


Figure E.1: An Image of Cross Section of the bar for the original wing before breakage

For the original wings, $c_1 = 0.243$ and $c_2 = 0.506$ are calculated using Eqn. E.1. Using results for c_1 and c_2 the individual inertial values $I_1=6.1E-5$ and $I_2 = 0.00489$ can be found by using Eqn. E.2. Then, Eqn. E.3 helps derive the total inertia (I_{tot}) to be, $I_{tot} = 0.0076 \text{ in}^4$. With this given information about inertial terms and by the knowledge of approximate force acting on a wing (100 N) and the length of a wing (1.2 m), moment acting on the wing can be calculated: $M=529.4\text{lb}\cdot\text{in}$. Now, alternating stresses can be calculated using Eqns. E.4 and E.5. Using these equations, $\sigma_a = 34.55\text{kpsi}$ and $\sigma_b = 16.62\text{kpsi}$. For the design purposes worst case scenario will be taken into account where alternating

stress is 34.55ksi . This value implies that the stress sustained by the material is too high, and it is very close to the maximal tensile strength (35ksi) that wing material can tolerate. This means that there is almost no safety factor (safety factor = 1.013). Low safety factor in turn implies that the wing will easily brake under any flapping cycle.

E.2 Analytical Fatigue Stress Analysis of the Reinforced Wing Design

In an attempt of fixing broken wings, wing structure was reinforced using additional aluminum angle bars. Reinforced wing cross section diagram is shown in Figure E.2.

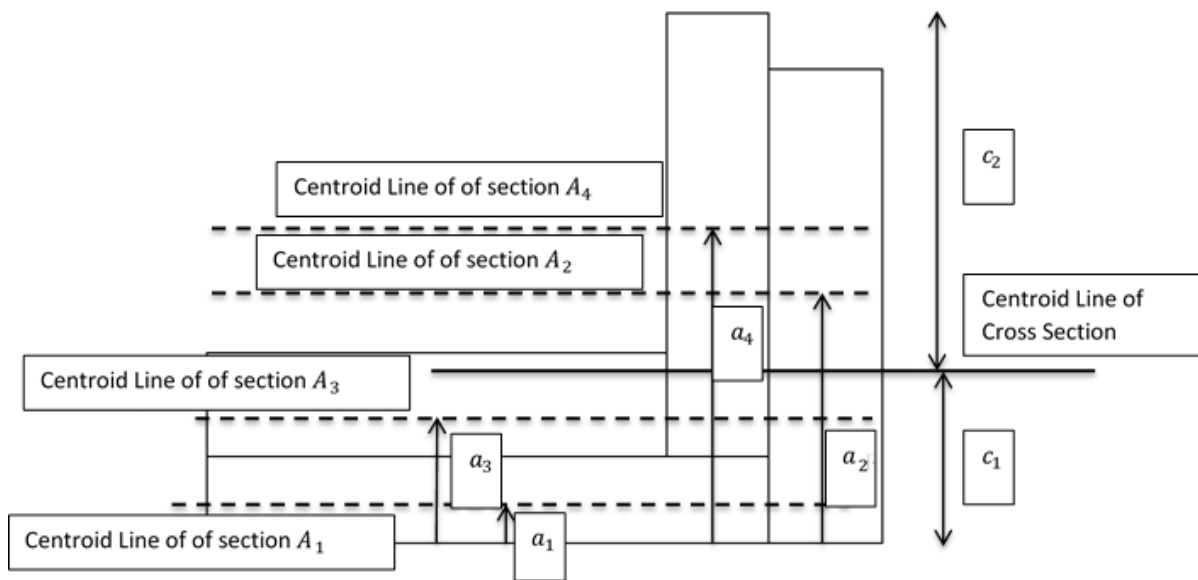


Figure E.2: A diagram of cross section of the bar for the reinforced wing

Using values from the previous calculations $c_1 = 0.225$ and $c_2 = 0.7248$. Using these numbers and Eqn. E.2, individual inertial terms for wing bars were found $I_1 = 1.017\text{E-}4$ and $I_2 = 0.004394$ $I_3 = 4.8828\text{E-}4$ $I_4 = 0.0089309$. Then using Eqn. E.3, total inertia was calculated to be: $I_{tot} = 0.02524\text{ in}^4$. Once deriving values for new inertial terms and using moment derived above ($M = 529.4\text{ lbf}\cdot\text{in}$) alternating stresses for the reinforced wings were calculated using Eqns. E.4 and E.5. Alternating stresses accounted for: $\sigma_a = 15.20\text{ksi}$ and $\sigma_b = 4.722\text{ksi}$. As the maximal alternating stress is 15.20ksi , and it is below the maximal tensile strength of the material (35ksi), significant number of cycles can be induced by flapping.

S-N graph

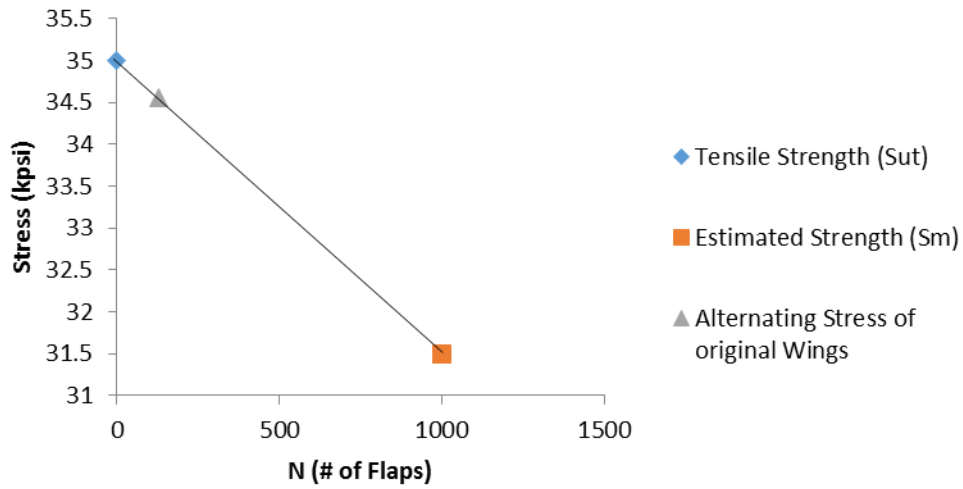


Figure E.3. An S-N graph showing alternating stress on the Original Wings

S-N Graph

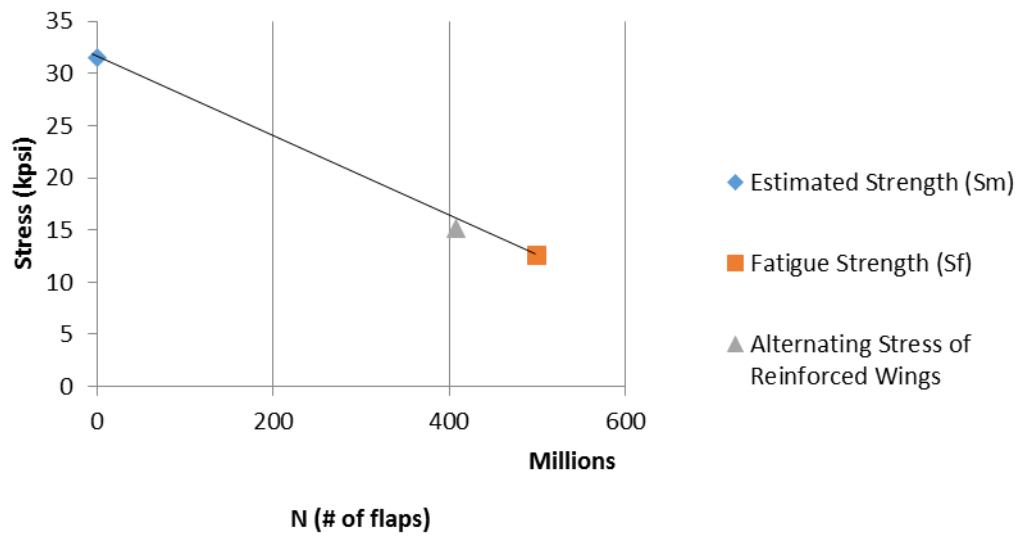
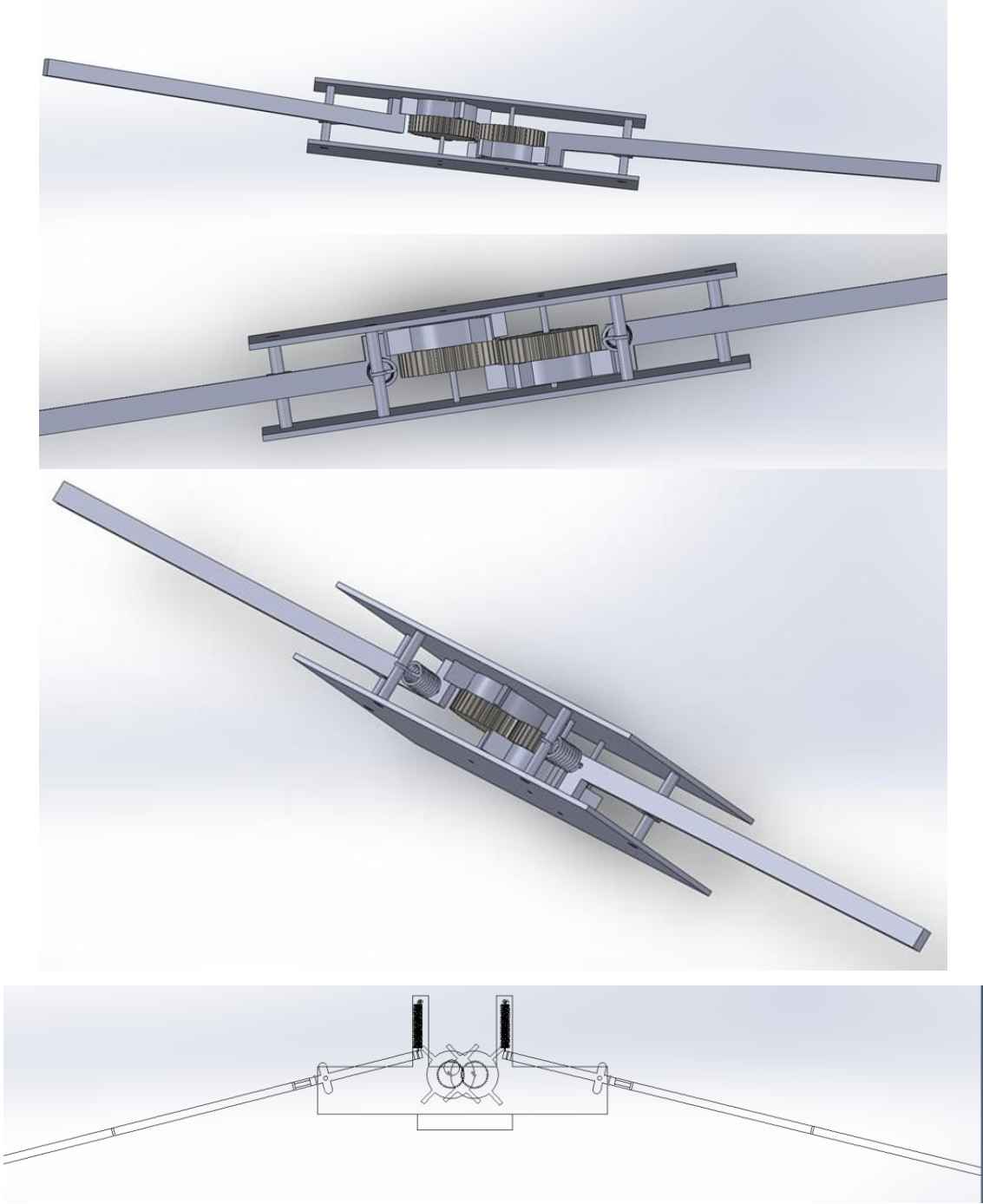


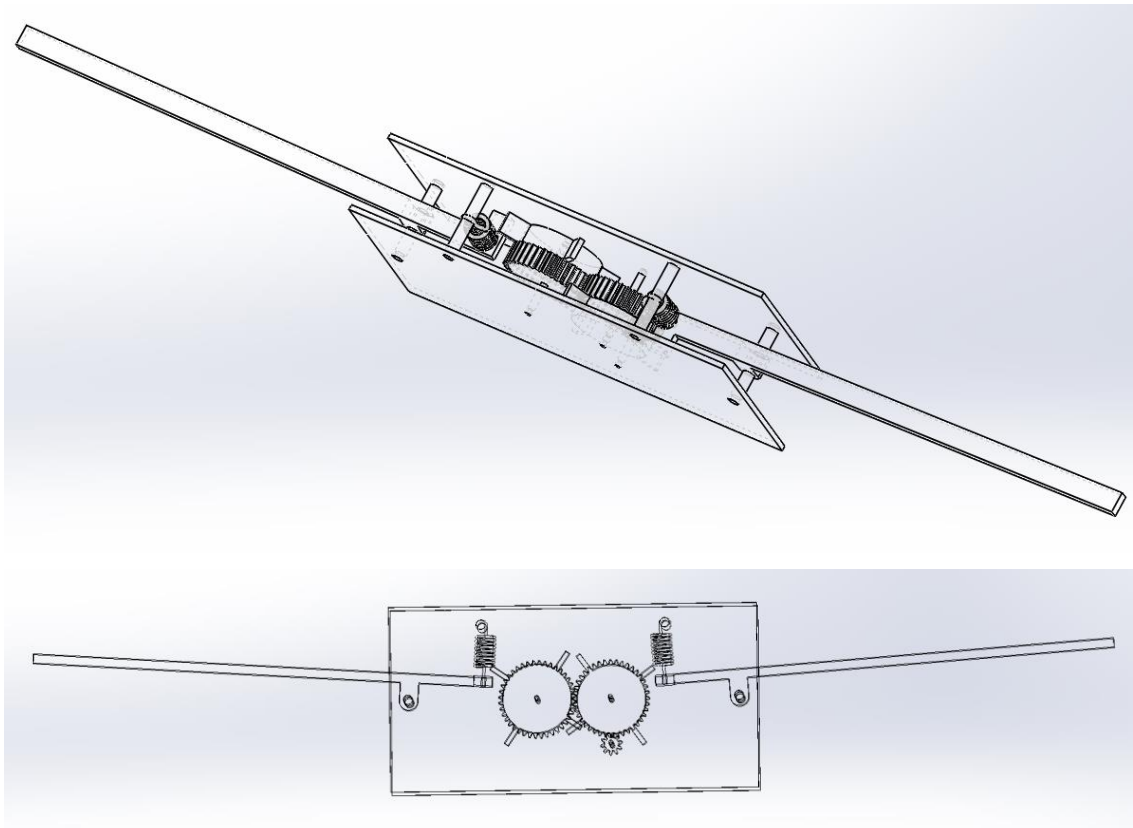
Figure E.4. An S-N graph showing alternating stresses on Reinforced Wings

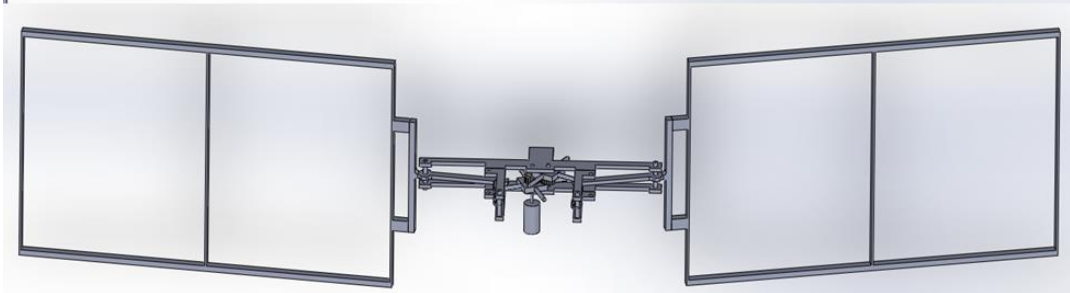
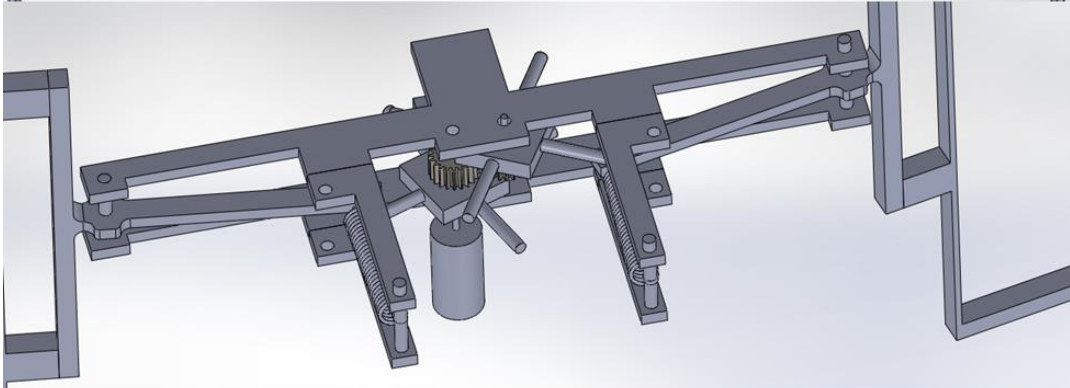
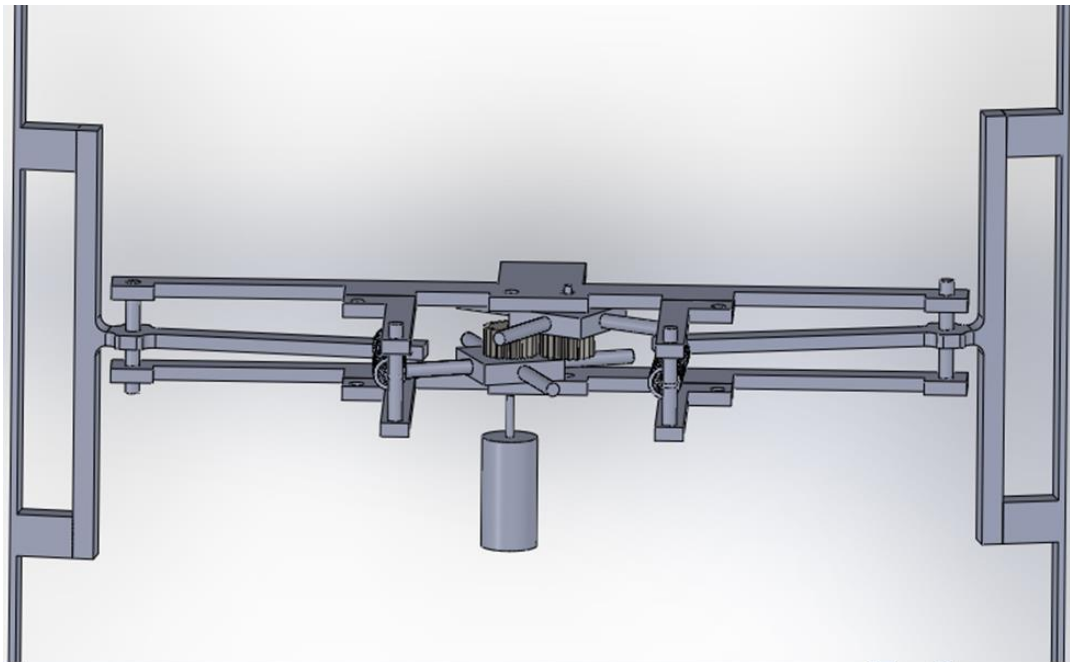
According to these calculations a safety factor is 2.07, which implies that reinforced wings can flap at least 10^3 times. According to the S-N graphs original wings can endure 128 flaps shown in

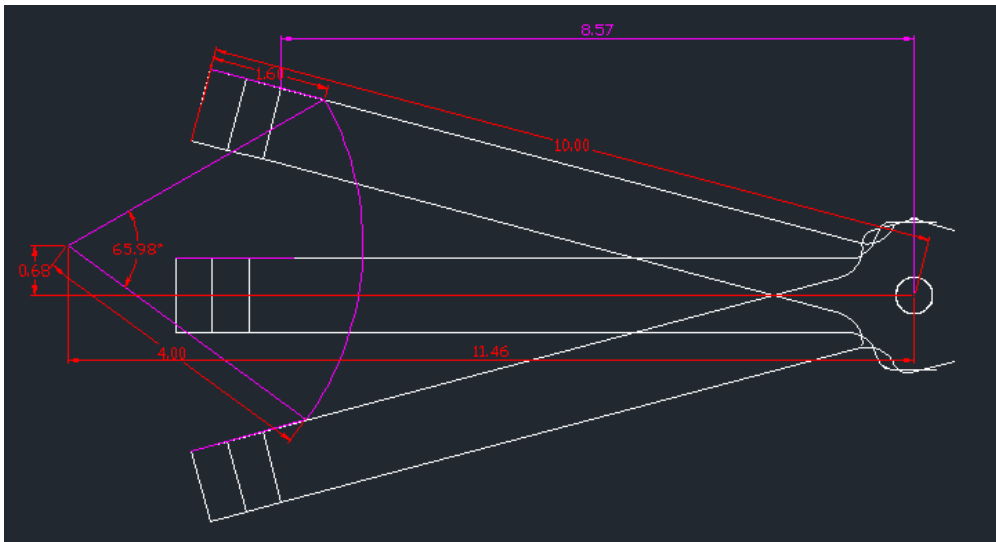
Figure E.3 and the reinforced wings can endure up to 408 million flaps as shown in Figure E.4. Due to the many assumptions during calculations, this is a very rough estimate of fatigue endurance of wing materials, and at least safety factor of 2 is required for assurance.

F.2 CAD Drawings of the Second Design and Other Parametric Simulations

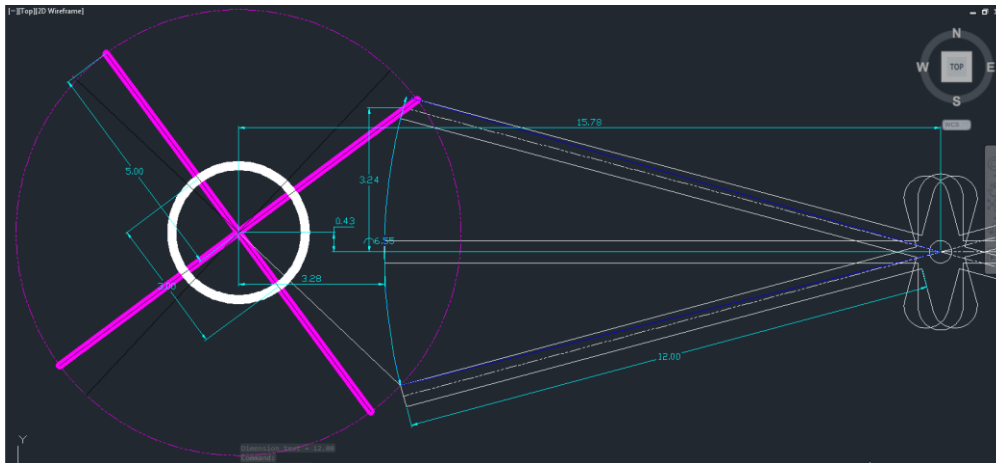




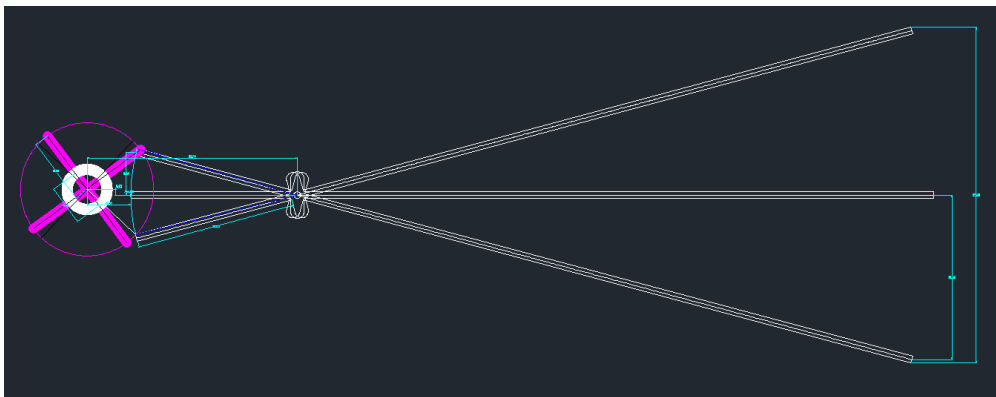




Required lengths and degrees for a paddle pushing a wing bone



Pink: paddle with 4 paddle sticks rotating and pushing the wing for downstroke

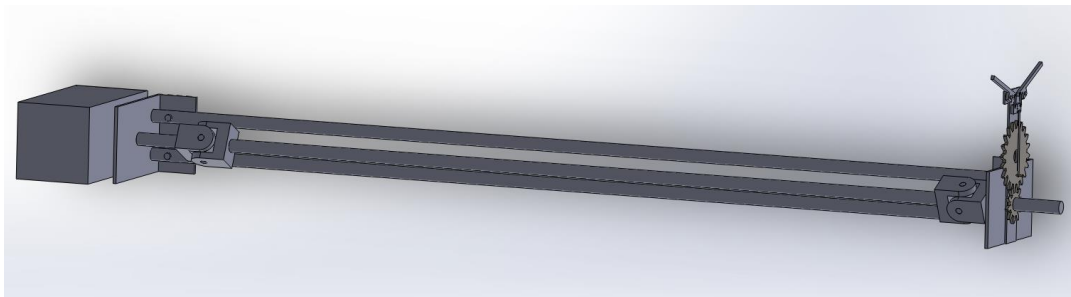


Entire wing trajectory

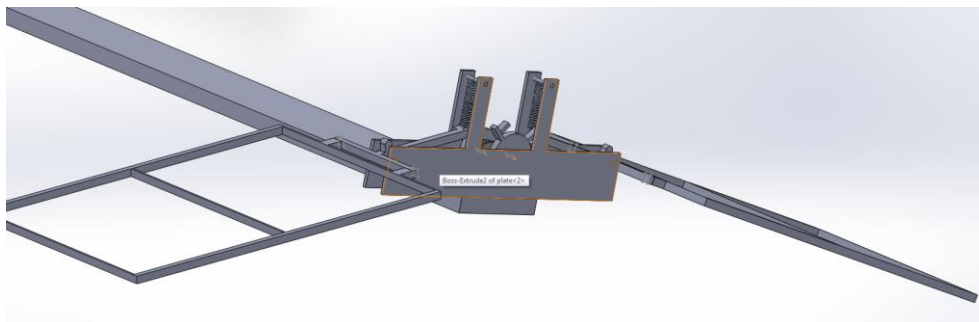
Appendix G: Alternative Designs Generated during the Design Process

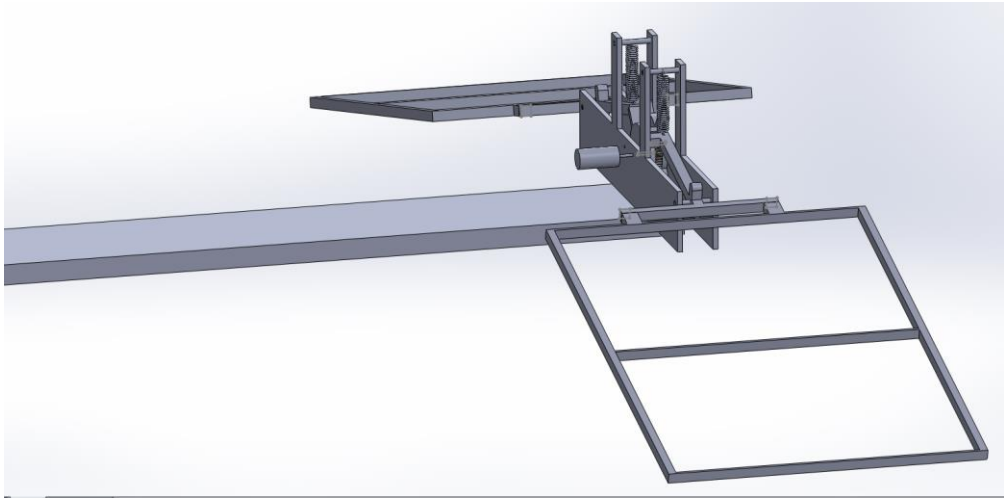
Our team came up with several alternative designs that were not actually made but they helped a great deal in developing an actual, final prototype

G.1 Conceptual design with rotating platform using universal joint



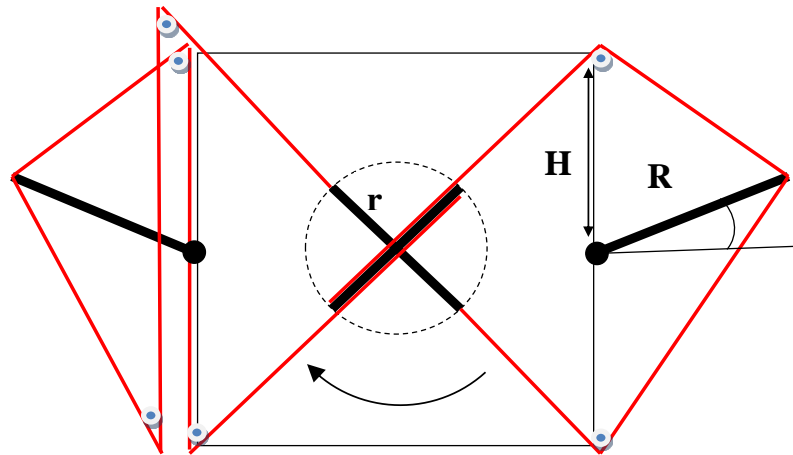
G.2 Second prototype with proposed counter balance











G.3 Proposal for the first prototype

Material: acrylic, rotary bearings, screws, rollers, hinges, fishing cable and one custom made crank



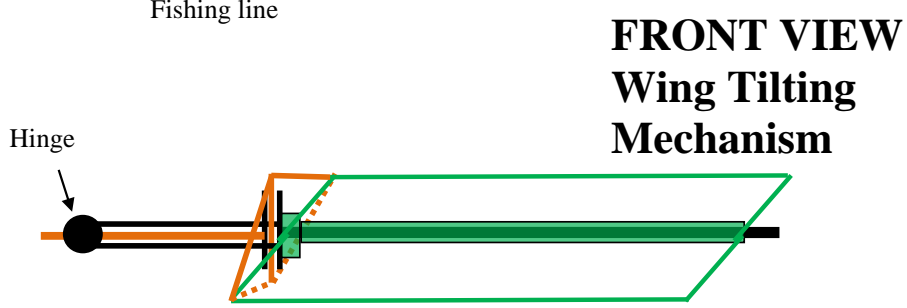
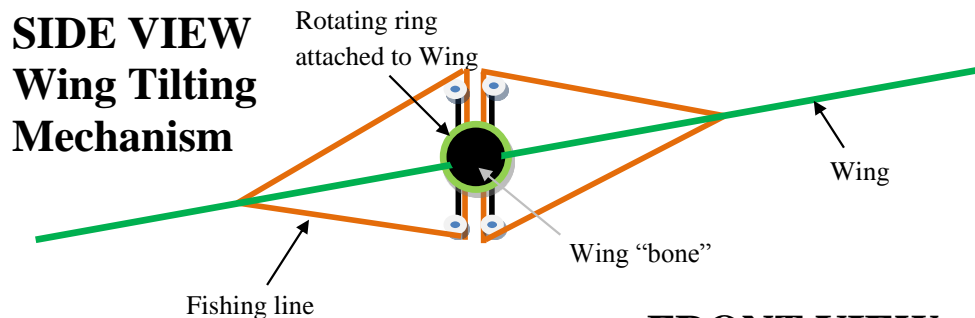
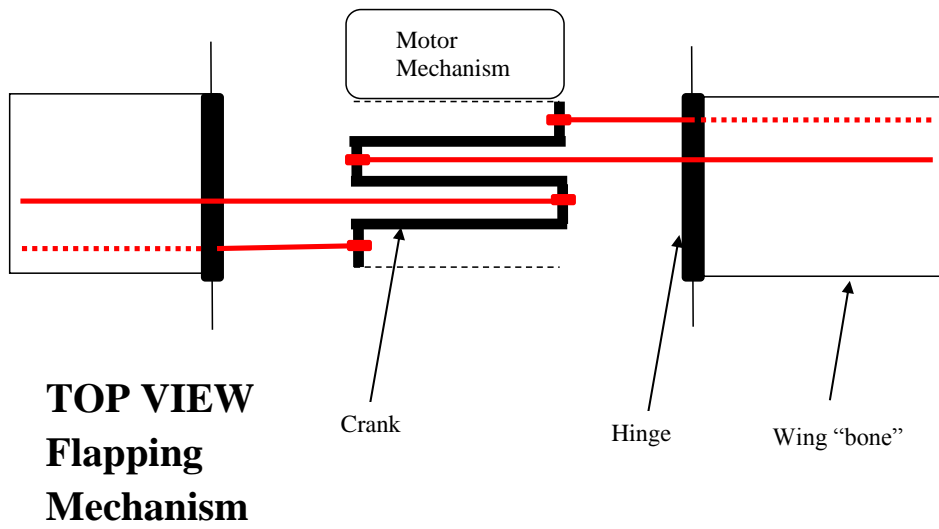
LEGEND FOR FRONT VIEW

-  Roller
-  Fishing line
-  Hinge
-  Wing "bone"
-  Crank
-  Disk (motor)

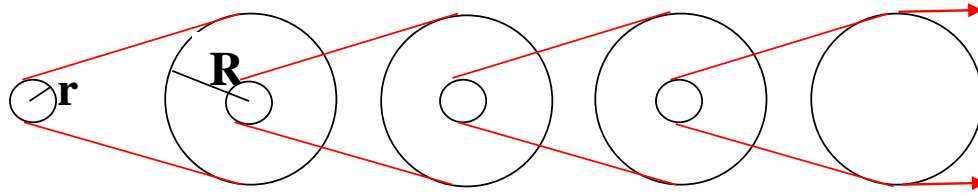
FRONT VIEW
Flapping
Mechanism

Maximal wing angle is

$$\sin \theta_{max} = \frac{r}{R} \sqrt{\frac{H^2 + R^2}{H^2 + r^2}}$$



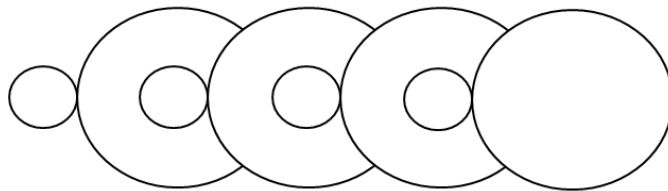
Wing tilting mechanisms can be cable (fishing line) driven. It will need very large torque output. The torque amplifier is sketched below.



The torque amplification in the above example is

$$\left(\frac{R}{r}\right)^4$$

Another torque amplification, that is more suitable for wing flapping mechanism as described above is with gear mechanism. The torque amplification is the same as in the above example.



G.4 Gigantic Flapping Wing Robot

Imagine platform in the form of three link arm with two constrained (“shoulder” and “elbow”) angles and wrist sliding on the vertical beam. Hence arm with just one degree of freedom that can be expressed in terms of wrist height. Wings mechanism, maybe similar to room size wings mechanism from term B but much larger, is attached to arm’s wrist and actuated by two cables that are aligned with arm. One cable is pulling one side (active during wings down-stroke) and the other cable is pulling bottom the other side (active during wings up-stroke) of the wing mechanism. Cables are enclosed within Bowden tubes to minimize friction and attached to two connected gears at the base of shoulder joint.

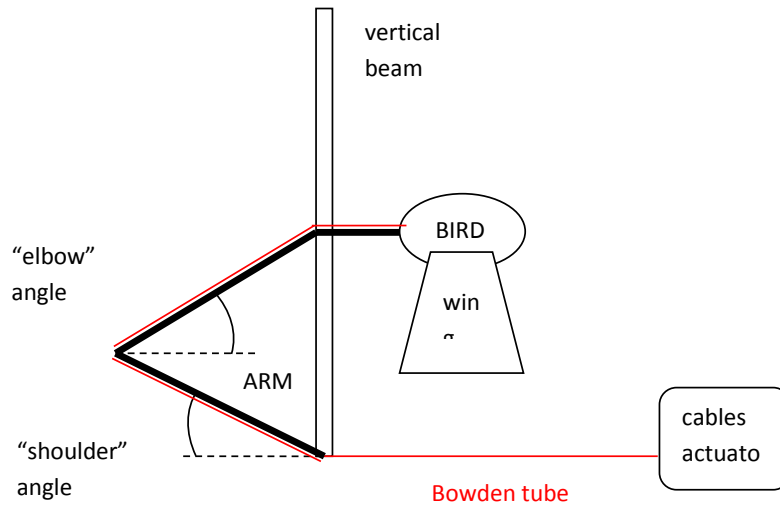
Rotation of gears causes 180 degrees out of phase linear motion of cables. The exact length of cables will be finely tuned. Also, cables will be added with elastic element in series. Hence, prototype will be robust to possible errors in cable lengths. If elastic elements are attached at the bottom, measurement of their length can provide information on input cable force. The gear mechanism will be actuated by powerful enough motor (e.g. car’s motor).

For slow wings' speed the wings mechanism will be located at minimal height (defined for example by stopper). As wings speed subsequently increases the wing mechanism will start to "take off" by increasing height, i.e. the "shoulder" and "elbow" angles will increase.

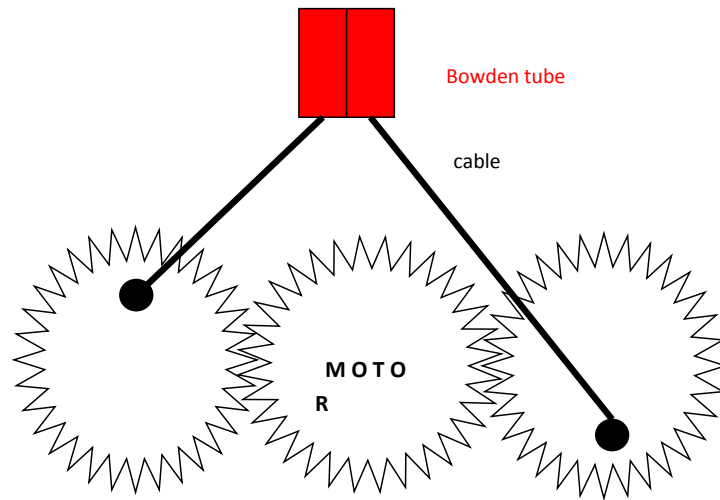
The mass of each element will be carefully measured beforehand. The motion will be then recorded with high speed camera and lift forces will be directly calculated. Additional mass can be added to wrist.

We need to make sure that cable actuation is not producing change in wrist height when there is no drag force due to flapping. In other words we need to make sure that wrist height change is due to drag forces and not cables forces that are simply transferred to arm. One way to do it is to attach spring instead of wings and confirm that. Probably the safest thing to do is to have cables pull in horizontal direction only.

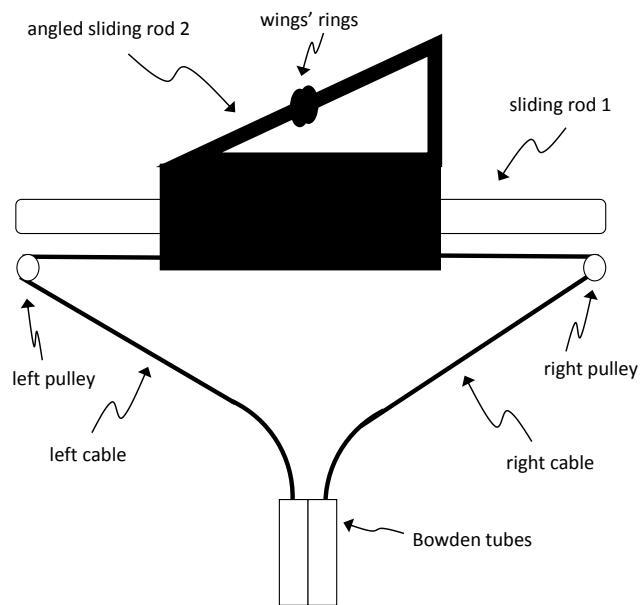
Drawings below illustrate some of these design ideas. Please suggest your own designs.



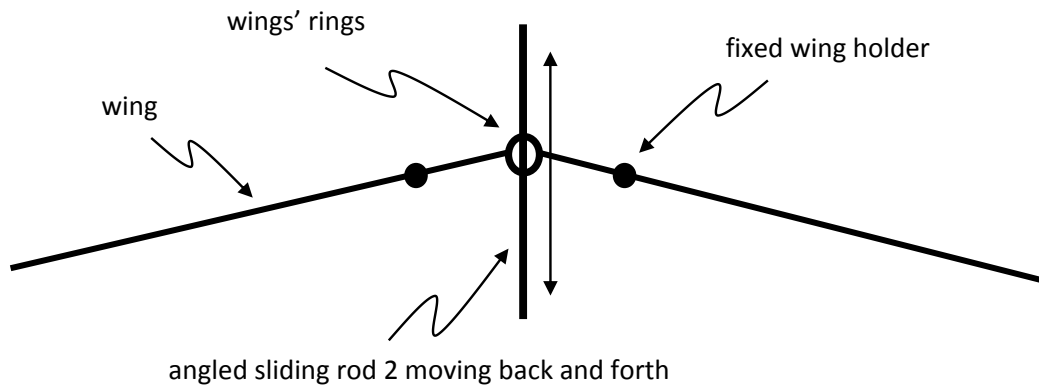
Cable actuator (e.g. car engine) causes motion of the wings. This motion causes drag induced lift forces that cause change in height of bird. In other words bird is flying in place. For equal lengths of "upper" and "lower" arm angles will be same.



Cable actuator: Cables attachments are out of phase and hence produce different cable lengths.

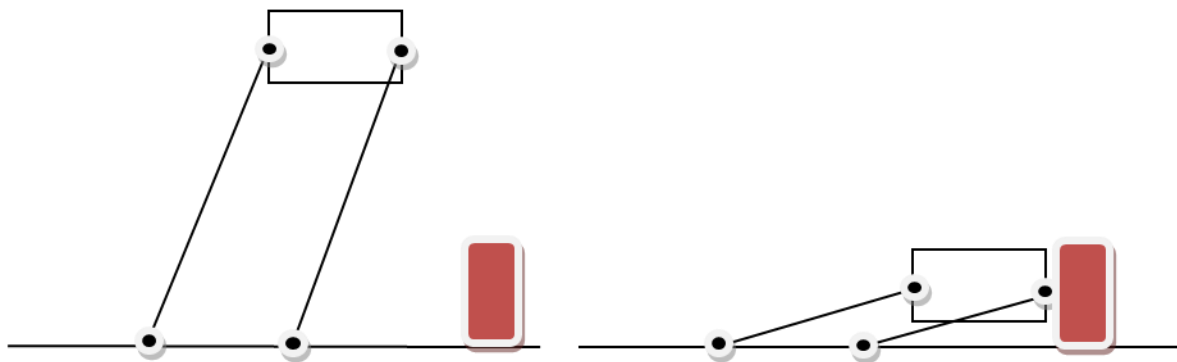


Horizontal motion within the wings' mechanism. Motion of cables cause motion of angled sliding rod 2 on top of sliding rod 1. Hence, horizontal cable forces actuate vertical motion of the wings rings.

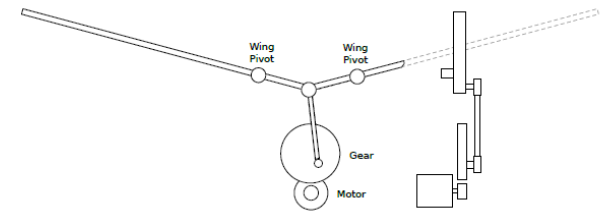
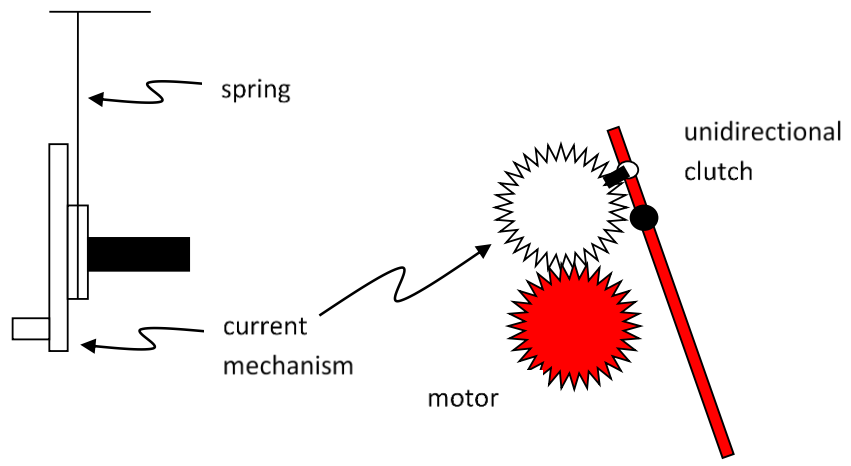


Vertical motion of the wings. Motion of the angled sliding rod into and out of page cause vertical motion of wings rings and hence vertical motion of wings.

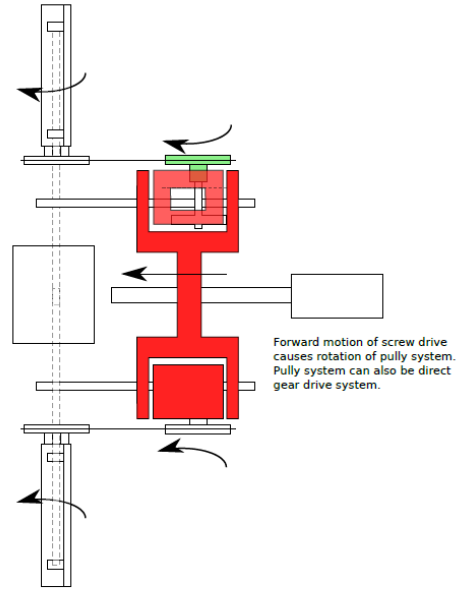
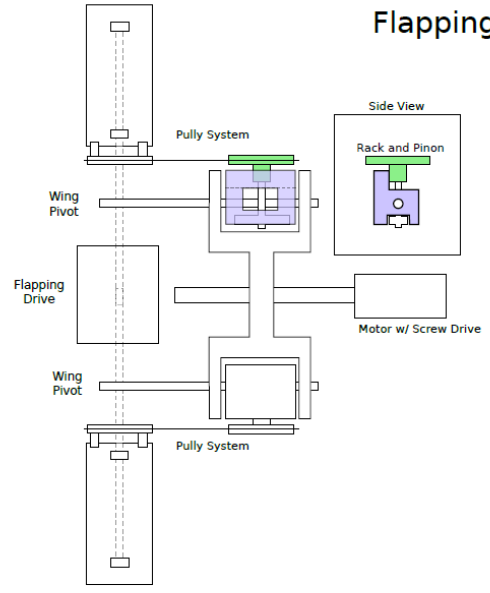
G.5 Proposal for second prototype



Two legs needed to keep bird orientation parallel to ground. Distance between feet needs to be equal to bird length (side view as shown above). Red unit on right is motor and unidirectional clutch. They could be both operated manually by operator. Bird carries only passive mechanism identical to small bird that you already built. The only difference is that there is spring attached to bird (wall of box) and main gear mechanism. The bird is charged by slowly storing potential energy in the elastic spring. When clutch is disengaged elastic potential energy will cause high power flapping. Flapping will last only second or two but that should be enough to collect valuable data. The longer the spring the more linear dynamical output will produce. We should maybe consider spring attachment point vertically far above the bird maybe even meter or two.



Flapping Drive



Wing Rotation Drive